1 **Combining Electromagnetic Induction and Satellite-based NDVI Data for Improved**

2 **Determination of Management Zones for Sustainable Crop Production**

4 **Authors**

5 Salar Saeed Dogar[1]*, Cosimo Brogi[1], Dave O'Leary[2,3], Ixchel M. Hernández-Ochoa[4], Marco

6 Donat[5,6], Harry Vereecken[1], and Johan Alexander Huisman[1]

7 [1] Agrosphere Institute (IBG-3), Forschungszentrum Jülich GmbH, 52425 Jülich, Germany

8 [2] Hy-Res Research Group, School of Natural Sciences, Earth and Life, College of Science and Engineering, University

9 of Galway, Galway, Ireland

10 [3] Teagasc, Animal and Grassland Research and Innovation Centre, Moorepark, Fermoy, Ireland

11 [4] Institute of Crop Science & Resource Conservation (INRES), Crop Science Group, University of Bonn, 53115 Bonn,

12 Germany

13 [5] Leibniz Centre for Agricultural Landscape Research, 15374 Müncheberg, Germany

14 [6] Faculty of Landscape Management and Nature Conservation, University for Sustainable Development (HNEE),

15 16225, Eberswalde, Germany

18 *Corresponding Author (s.dogar@fz-juelich.de)

Abstract

Accurate delineation of management zones is essential for optimizing resource use and improving yield in precision agriculture. Electromagnetic induction (EMI) provides a rapid, non-invasive method to map soil variability, while the Normalized Difference Vegetation Index (NDVI) obtained with remote sensing captures above-ground crop dynamics. Integrating these datasets may enhance management zone delineation but presents challenges in data harmonization and analysis. This study presents a workflow combining unsupervised classification (clustering) and statistical validation to delineate management zones using EMI and NDVI data in a single 70 ha field of the patchCROP experiment in Tempelberg, Germany. Three datasets were investigated: (1) EMI maps, (2) NDVI maps, and (3) a combined EMI-NDVI dataset. Historical yield data and soil samples were used to refine the clusters through statistical analysis. The results demonstrate that four EMI-based zones effectively captured subsurface soil heterogeneity, while three NDVI-based zones better represented yield variability. A combination of EMI and NDVI data resulted in three zones that provided a balanced representation of both subsurface and above-ground variability. The final EMI-NDVI derived map demonstrates the potential of integrating multi-source datasets for field management. It provides actionable insights for precision agriculture, including optimized fertilization, irrigation, and targeted interventions, while also serving as a valuable resource for environmental modelling and soil surveying.

1 Introduction

Reliable and accurate agricultural management zones that capture within-field variability affecting crop development can play a pivotal role in sustainable agriculture. Management zones can be used in the context of precision agriculture to optimize farming practices, increase yields, and reduce the use of available resources (Gebbers and Adamchuk, 2010; Janrao et al., 2019). This is not only valuable for profit maximization (Adhikari et al., 2022), but is also vital to meet future climate change and food security challenges (Antle et al., 2017; Chartzoulakis and Bertaki, 2015; Bongiovanni and Lowenberg-Deboer, 2004), such as Goal 2 (Zero Hunger) and Goal 15 (Life on Land) of the United Nations Sustainable Development Goals (SDGs) (Hou et al., 2020; UN, 2021). Generally, management zones aim to consider the impact of various factors that can influence crop productivity and result in yield gaps, a key one being soil heterogeneity and health (Licker et al., 2010). Soil systems can be relatively static in time (Arshad et al., 2015) and are fundamental due to their multifunctional role and impact on ecosystem services (Hamidov et al., 2018). Within these systems, soil properties such as texture, organic matter content, cation exchange capacity, and bulk density greatly influence soil moisture dynamics, salinity, nutrient availability, and other variables affecting crop yield (Kibblewhite et al., 2008; Dobarco et al., 2021) and are thus a good target for management zone delineation. However, soil heterogeneity is not solely responsible for yield losses, and effective management zones should also incorporate other influencing factors to provide a comprehensive and holistic management solution.

Traditional methods for soil characterization to support management zone delineation (Brogi et al., 2021; Geologischer Dienst NRW) generally rely on laborious in-situ sampling and laboratory analysis, which may fail in capturing soil variability with sufficient detail (Kuang et al., 2012). In

recent years, advances in proximal soil sensing, defined as methods that utilize sensors positioned near or in direct contact with the soil (Adamchuk et al., 2017), have provided valid alternatives to direct soil sampling (Pradipta et al., 2022). In particular, non-invasive agro-geophysical methods such as electromagnetic induction (EMI) have proven suitable for management zone delineation due to their high mobility (Binley et al., 2015; Garré et al., 2021) and the fact that the measured apparent electrical conductivity (ECa) of the soil is related to key soil properties, such as soil salinity, soil water content, texture, compaction, and organic matter content (Corwin and Lesch, 2003; Abdu et al., 2008; Altdorff et al., 2017; Jadoon et al., 2015; Robinet et al., 2018; Zhu et al., 2010; von Hebel et al., 2018). Modern EMI devices are able to efficiently provide soil information for multiple depth ranges thanks to multi-coil instrumentation (Rudolph et al., 2015; von Hebel et al., 2014; Blanchy et al., 2024; Lueck and Ruehlmann, 2013; Corwin and Scudiero, 2019), especially when supported by a moderate amount of ground truth data (Brogi et al., 2019). However, the use of EMI alone can show limitations in capturing local aspects that have an impact on yield but that are not strongly influenced by soil variability. For instance, pest and weed infestations can drastically reduce crop productivity, and these factors may not correlate directly with soil variability (Becker et al., 2022; López-Granados, 2011). Additionally, climate change impacts, such as altered precipitation patterns and temperature fluctuations, can affect crop health and yield in ways that EMI cannot detect (Pradipta et al., 2022). Finally, it is also important to stress that accurate EMI mapping generally requires optimal conditions like bare soil, favourable weather, and absence of confounding factors (James et al., 2003).

An alternative to proximal soil sensing for the delineation of management zones is the use of remote sensing approaches, which enables efficient large-scale data acquisition without the need

91   for direct physical access to the investigated area (Weiss et al., 2020). By using sensors mounted

92   on satellites, airplanes, or drones, remote sensing monitors parameters related to crop health and

93   development (Jin et al., 2019; Liaghat and Balasundram, 2010). For example, vegetation indices

94   such as the Normalized Difference Vegetation Index (NDVI) are generally well-established,

95   simple, and effective proxies for crop health (Carfagna and Gallego, 2005; Stamford et al., 2023;

96   Wang et al., 2020; Xue and Su, 2017). High-resolution (<5 m) data products from satellites are

97   being increasingly used in precision agriculture (Mohammed et al., 2020; Trivedi et al., 2023).

98   Also, remote sensing platforms like PlanetScope, Sentinel-2, and Landsat offer frequent revisit

99   times, thus providing sufficient temporal resolution to track changes in plant health throughout the

100   growing season (Hunt et al., 2019; Skakun et al., 2021). Despite these advantages, remote sensing

101   data are affected by cloud cover or other sub-optimal meteorological conditions (Wilhelm et al.,

102   2000) and primarily capture above-ground information on plant health and biomass, and can thus

103   struggle to provide direct information about the interplay between soil conditions and crop

104   development.

105

106   Several studies have explored a combination of EMI and remote sensing methods for the

107   delineation of management zones. For example, von Hebel et al. (2021) combined EMI and drone-

108   based NDVI measurements and found that EMI-based management zones offered consistent

109   insights into soil texture and water content, while the added value of NDVI strongly depended on

110   the timing of the drone measurements and thus on the specific crop conditions. In a similar study,

111   Esteves et al. (2022) showed that integration of EMI and NDVI from Sentinel-2 (10 m resolution)

112   effectively provided zones with distinct soil and crop nutrient characteristics. However, they

113   reported a negative relationship between ECa and NDVI due to local magnesium imbalances and

114 vegetation stress. In addition to EMI and remote sensing, historical yield maps can help in

115 identifying yield trends across years and different cultivated crops. For example, Ali et al. (2022)

116 integrated seven years of yield data with Landsat-based NDVI and soil sampling over a 9 ha field,

117 but ultimately could obtain only a limited subdivision of the field into two management zones with

118 a relatively low resolution of 30 m. Overall, previous studies have made important contributions

119 towards integrating EMI and NDVI data for improved management zone delineation (Corwin and

120 Scudiero, 2019; Ciampalini et al., 2015). However, the results can be influenced by data resolution

121 and acquisition timing as well as by local management and soil-plant interactions, with some

122 studies suggesting that EMI alone can offer sufficient insights into soil patterns (Esteves et al.,

123 2022; von Hebel et al., 2021). Nonetheless, the added value of NDVI holds unexplored potential

124 due to the higher spatial and temporal resolution of recent satellite platforms (Breunig et al., 2020;

125 Georgi et al., 2018).

126

127 Machine learning clustering algorithms have been widely used to delineate management zones

128 from spatially distributed datasets such as EMI or NDVI (Saifuzzaman et al., 2019; Castrignanò

129 et al., 2018; Chlingaryan et al., 2018; Zhang and Wang, 2023). For example, Wang et al. (2021)

130 used supervised Random Forest classification for combining EMI data with environmental

131 covariates to predict soil salinity. Similarly, Brogi et al. (2019) employed supervised learning to

132 combine EMI with soil sampling and generate high-resolution soil maps for a 1 km² agricultural

133 area. However, the results of supervised classification approaches may depend on the interpreter

134 and often need expert knowledge as well as extensive ground-truth data for training (Liakos et al.,

135 2018; Usama et al., 2019). K-means and ISODATA clustering are unsupervised methods used to

136 delineate management zones (Bijeesh and Narasimhamurthy, 2020; Ylagan et al., 2022; Tagarakis

137 et al., 2013) but these approaches can be sensitive to initial conditions and struggle to handle non-

138 linear relationships in datasets (Geng et al., 2020; Li et al., 2018). Thus, more advanced methods

139 such as self-organizing maps (SOM) have been successfully used to analyse complicated data

140 structures provided by proximal and remote sensing data (Romero-Ruiz et al., 2024; Moshou et

141 al., 2006; Taşdemir et al., 2012). A remaining key challenge of unsupervised methods is the

142 definition of the optimal number of clusters. Widely used approaches such as the elbow and

143 silhouette method (Saputra et al., 2020) often struggle when applied to non-linearly distributed or

144 spatially complex datasets (Schubert, 2023), and may thus require subjective judgment or expert

145 knowledge (Liang et al., 2012). To address this challenge, the Multi-Cluster Average Standard

146 Deviation (MCASD) approach that relies on an evaluation of the intra-cluster variability has

147 recently been introduced (O'Leary et al., 2023) and successfully applied to the integration of

148 complex spatial datasets (O'Leary et al., 2024). However, many of these novel approaches have

149 seen limited applications in agricultural contexts (Khan et al., 2021) and the added value of

150 delineating management zones from datasets of different origin remains unaddressed (Koganti et

151 al., 2024).

152

153 Within this context, this study expands on previous research by combining high- resolution multi-

154 coil EMI and satellite-based NDVI data within a harmonized framework, applying consistent

155 normalization, and validating the resulting zones with multi-year yield data and dense soil

156 sampling. The potential of delineating management zones by integrating EMI and NDVI is

157 explored for a single 70 ha agricultural field near Berlin, Germany. Management zones were

158 derived using three data sources: i) ECa maps from nine different depths of investigation (DOI)

159 obtained with EMI between 2022 and 2024, ii) seven NDVI images obtained from PlanetScope in

160 2019, and iii) a combination of EMI and NDVI data. Management zones were delineated using

161 SOM while the optimal number of clusters was obtained with the MCASD method. In a following

162 step, the number of clusters was refined using post-hoc analysis using a large dataset of soil

163 samples and yield maps at 10 m resolution from 2011 to 2019. Finally, it was evaluated to what

164 extent management zones derived from EMI, NDVI, or a combination of both represent soil

165 characteristics and yield patterns using visual inspection and statistical analysis.

166

167 **2 Materials and Methods**

168 **2.1 Study area**

169 The study site is part of the patchCROP (patchCROP, 2020) landscape laboratory of the Leibniz

170 Centre for Agricultural Landscape Research (ZALF) near Tempelberg, Brandenburg, Germany

171 (52.4426 N, 14.1607 E, altitude 68 m). It is located in the transition zone between humid oceanic

172 and dry continental climate. The long term average temperature from 1980 to 2020 was 8.3°C and

173 the mean annual precipitation for the same period was 533 mm (DWD, 2021; Koch et al., 2023).

174 The investigated field has an area of approximately 70 ha (Figure 1). Until 2020, this field was

175 managed as a single unit. In March 2020, the patchCROP experiment was established to study the

176 impact of landscape diversification through the use of smaller field sizes, site-specific crop

177 rotations, different field management practices, and the use of new technologies including

178 proximal soil sensing, remote sensing, and robotic technologies (Grahmann et al., 2021). For this,

179 thirty patches of 72 x 72 m were established within the investigated field (Donat et al., 2022) (Fig.

180 1). In terms of geomorphology, the site is described as a young moraine landscape shaped by past

181 glaciations, and characterized by an undulating relief and heterogeneous soil characteristics (Koch

182   et al., 2023; Öttl et al., 2021; Meyer et al., 2019). The topsoil is predominantly sandy, but a more

183   clayey layer is present at different depths in the subsoil (Hernández-Ochoa et al., 2024).

184
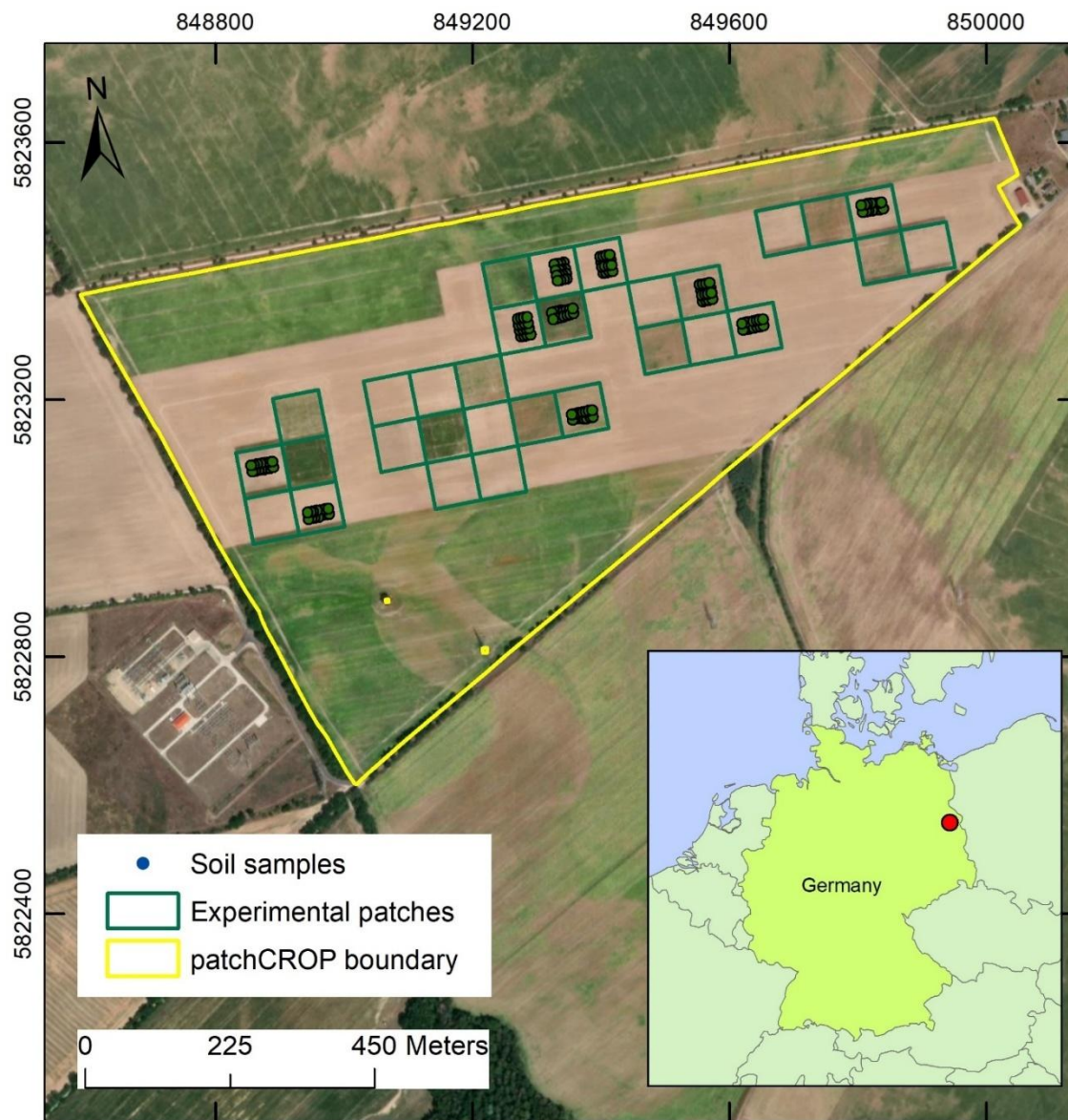
185   Figure 1. Overview of the patchCROP study area in Tempelberg, Brandenburg (ESRI, 2020). The

186   yellow border indicates the boundary of the investigated field, whereas the green boxes indicate

187   the thirty patches of the patchCROP landscape experiment. The inset map shows the location of

188   the study site within Germany; the red dot indicates the site location in Tempelberg.

189

2.2 Data collection and processing

The overall methodology of this study is summarized in Figure 2. This flowchart highlights the

role of EMI and NDVI datasets in the clustering process and the use of multi-year yield maps and

soil samples for validation and refinement of the resulting management zones. More details are

provided in the subsequent sections.

195

196

197

198

199
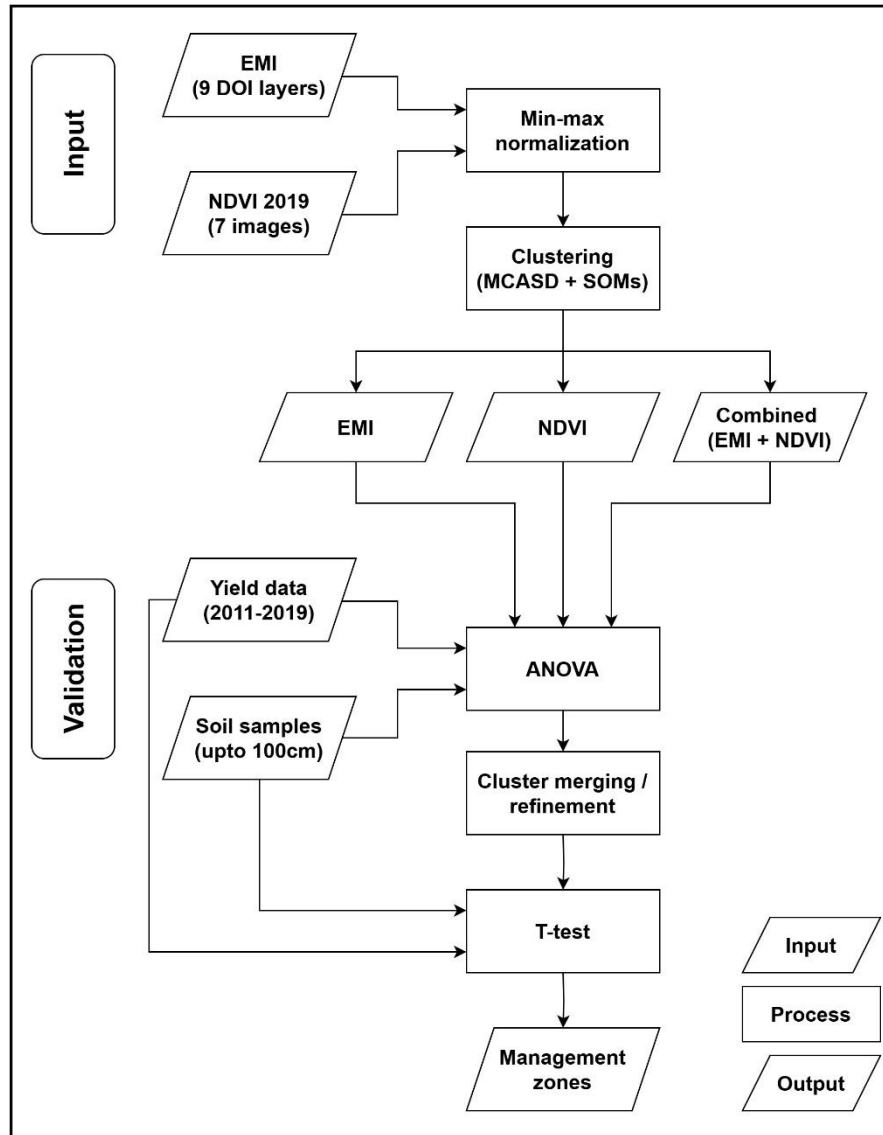
Figure 2. Workflow diagram showing the integration of proximal (EMI) and remote sensing (NDVI) data for unsupervised clustering using MCASD and SOMs. Yield and soil datasets were used for post-hoc validation and refinement of management zones.

2.2.1 Electromagnetic Induction (EMI) measurements

Frequency-domain EMI devices generate a fixed-frequency alternating current in a transmitter coil, which produces a primary magnetic field. This primary magnetic field induces eddy currents in the soil, thus generating a secondary magnetic field. The primary and secondary magnetic fields

207   are sensed by a receiver coil. The quadrature component of the ratio between the primary and

208   secondary magnetic fields is directly proportional to the apparent electrical conductivity (ECa) of

209   the ground (Keller and Frischknecht, 1966; Ward and Hohmann, 1988; McNeill, 1980). The

210   measured ECa is strongly affected by soil properties such as salinity, water content, clay content

211   (and thus texture), compaction, and to a lesser degree organic matter content and cation exchange

212   capacity (Corwin and Lesch, 2005; Robinet et al., 2018). The depth sensitivity of EMI

213   measurements depends on coil spacing and coil orientation. Larger spacing results in increased

214   depths of investigation (DOI), while the coil orientation influences the sensitivity to shallow or

215   deep subsurface (Lavoué et al., 2010; Simpson et al., 2009).

216

217   In this study, two EMI devices were used simultaneously: a CMD-Mini Explorer (GF Instruments,

218   Brno, Czech Republic) with three receiver coils oriented in a vertical coplanar configuration

219   (VCP), and a custom-made CMD-Mini Explorer – Special Edition equipped with six receiver coils

220   oriented in a horizontal coplanar configuration (HCP). The VCP configuration is most sensitive to

221   the shallow subsurface, with decreasing sensitivity as depth increases. In contrast, the HCP

222   configuration is less sensitive to the shallow subsurface, with sensitivity peaking at a depth of

223   approximately 0.4 times the coil separation (McNeill, 1980). As a rule of thumb, the DOI for the

224   VCP setup is approximately 0.75 times the coil separation. For the HCP setup, the DOI is

225   approximately 1.5 times the coil separation. For the set-up used here, the resulting DOI ranges

226   from 0-24 to 0-270 cm. Details of the EMI set-up are summarized in Table 1.

227

Table 1. Details of the two EMI devices with coil number, orientation, separation, DOI, and frequency.

EMI device	Receivers	Orientation	Separation (cm)	DOI (cm)	Frequency (Hz)
Mini Explorer	3	VCP	32	0-24	30
		VCP	71	0-53	
		VCP	118	0-89	
Mini Explorer	6	HCP	35	0-52	25.17
Special Edition		HCP	50	0-75	
		HCP	71	0-108	
		HCP	97	0-146	
		HCP	135	0-203	
		HCP	180	0-270	

Due to the ongoing PatchCROP experiment with small patches using variable cropping systems, it was not possible to cover the entire field in a single EMI campaign. EMI data were thus collected in four campaigns conducted between August 2022 and October 2024. During each campaign, the EMI devices were placed in sleds and warmed up for approximately 30 minutes before use. The sleds were then pulled by an all-terrain vehicle (ATV) at a speed of approximately 6 to 8 km/h. Data collection occurred at a frequency of 0.2 s, resulting in an inline spatial resolution of 0.25 to 0.50 m. A track spacing of ~2.5 m was used within the experimental patches and a track spacing between 5 to 45 m (typically well below 10 m) was used in the rest of the field. A Real Time eXtended (RTX) center point differential global positioning system (DGPS) (Trimble Inc., Sunnyvale, United States) was used to record the position of the sleds with centimeter accuracy.

241 For more information about the setup for EMI measurements, the reader is referred to von Hebel

242 et al. (2018).

243

244 The measured ECa values were filtered using a Python-based method similar to the approach of

245 von Hebel et al., (2014), which has been successfully applied in several studies (Brogi et al., 2019;

246 von Hebel et al., 2021; Kaufmann et al., 2020; Schmäck et al., 2022). The first filter removes

247 values that are deemed too high or too low based on user-defined thresholds (-50 and 50 mS/m in

248 this study). A second filter divides the data into a user-defined number of bins (20 in this study)

249 and removes the data from bins with a low fraction of measurements (<1% in this study). In a third

250 step, a spatial filter is used to identify and discard ECa values that deviate from adjacent positions

251 more than a given amount (1 mS/m in this study) to avoid unrealistically high lateral ECa

252 variations. After the application of these three filters, ~5% of the measured ECa values were

253 removed, although this value varied between measurement campaigns.

254

255 Given that the EMI data were acquired in four campaigns with different environmental conditions

256 (e.g. soil water content, soil temperature), each EMI acquisition campaign was separately

257 normalized by using a standardized z-score normalization method as used by Rudolph et al. (2015):

258

259 $ECa_{z,i} = (ECa_i - \mu_i)/\sigma_i$ (1)

260

261 where $ECa_{z,i}$ is the normalized ECa value for the i-th campaign, ECa_i is the measured ECa value

262 for the i-th campaign, μ_i is the mean ECa value of the i-th campaign, and σ_i is standard deviation

263 of ECa values for the i-th campaign. Following normalization, manual cleaning was conducted in

264 ArcMap v10.8.2 (ESRI, Redlands CA, USA) to remove points typically occurring at the start and

265 end of each campaign or in short periods where the EMI system was left stationary. In the final

266 step, the normalized data for each of the nine coil configurations were interpolated to a regular 3

267 by 3 m grid using ordinary Kriging with a gaussian semivariogram and merged into a single

268 multidimensional raster mosaic dataset.

269

270 **2.2.2 Remotely sensed NDVI data**

271 High-resolution PlanetScope Level 3B satellite images from the 2019 growing season (winter rye)

272 were used to obtain NDVI maps. Between 01-Jan-2019 and 31-July-2019, 48 cloud free images

273 were available. Seven of these images were selected to represent crop development during the

274 growing season. PlanetScope image products are pre-processed and have already undergone

275 radiometric and atmospheric corrections. No additional pre-processing was required. The

276 PlanetScope sensor captures spectral information in four bands: blue (B1), green (B2), red (B3),

277 and near-infrared (NIR - B4) with a spatial resolution of 3 m. The normalized difference vegetation

278 index (*NDVI*) was calculated using the reflectance in the red (*R*) and near-infrared bands (*NIR*):

279

280 $NDVI = (NIR - R)/(NIR + R)$ (2)

281

282 The resulting NDVI values range from -1 to 1, where values close to 1 indicate healthy vegetation,

283 and values close to zero or negative values generally represent non-vegetated surfaces, senescent,

284 stressed or unhealthy plants or dry vegetation, or features such as clouds and water that exhibit

285 lower NIR reflectance (Sishodia et al., 2020).

286

2.2.3 Yield data

Georeferenced yield maps of nine growing seasons (2011-2019) were used. These yield maps were generated using a yield monitoring system (CLAAS Quantimeter, Hersewinkel, Germany) mounted on two different combine harvesters. From 2011 to 2013, data were collected using a CLAAS 580. From 2014 onwards, a CLAAS Lexion 770 TT was used. In the 2011 – 2019 period, the field was either cultivated with winter rye (2011, 2013, 2014, 2016, 2017, and 2019) or rapeseed (2012, 2015, and 2018). For additional details on data processing and yield map generation, readers are referred to Donat et al. (2022). The original yield data from Donat et al. (2022) were available as georeferenced yield data points with a spacing of ~10 m. These points were interpolated to a regular grid with 10 m resolution using ordinary kriging.

2.2.4 Soil sampling and data on soil characteristics

Extensive soil sampling campaigns were conducted between 2020 and 2024, focusing on the experimental patches within the 70 ha field. At 160 locations, soil samples up to 100 cm depth were obtained using a Pürckhauer soil auger with an 18 mm inner diameter. The soil properties analyzed in this study included the depth of soil texture transition, defined as the depth (in cm) at which the sandy top layer ends (EOS (end of sandy layer) in the following), as well as the soil texture (percentage of sand, silt, and clay) of the top sandy layer and the layer below. Soil texture was determined by using the wet sieving and sedimentation method (ISO, 2002). The particle size distribution was defined according to the IUSS Working Group 150 WRB guidelines (IUSS Working Group, 2015). When multiple subsamples for a single layer were available at a given location, weighted averages of sand, silt, and clay fraction for the whole layer were obtained using the thickness of each subsample.

310

2.3 Clustering for delineation of management zones

Three different data combinations were created and investigated: a) EMI maps, b) time-series of

NDVI maps, and c) a combination of the EMI maps and NDVI maps. Before clustering, a standard

preprocessing step of normalization was applied on each dataset to ensure that variables with

different ranges and units contribute equally in the classification process. The choice of

normalization method can be particularly important when combining datasets with different scales,

such as EMI and NDVI, to prevent dominance of one dataset over the other and to maintain the

integrity of the input features In this study, a min-max scaling was applied, where all values were

rescaled to a standard range between 0 and 1 (Patro and Sahu, 2015). For EMI, a single

normalization was applied to the nine ECa_z maps. In this case, the min-max normalization used

the minimum ($ECa_{z\,min}$) and maximum value ($ECa_{z\,max}$) from all nine 9 maps:

$$ECa_z' = \frac{ECa_z - ECa_{z\,min}}{ECa_{z\,max} - ECa_{z\,min}} \tag{3}$$

where ECa_z is the original value, and ECa_z' is the normalized value. For NDVI, each of the seven

NDVI maps was normalized independently:

$$NDVI'_i = \frac{NDVI_i - NDVI_{i,min}}{NDVI_{i,max} - NDVI_{i,min}} \tag{4}$$

where $NDVI'_i$ is the normalized value for the i-th map, $NDVI_i$ is the original value of NDVI of the

i-th map, $NDVI_{i,\,min}$ and $NDVI_{i,\,max}$ are the minimum and maximum values of the i-th NDVI map.

This difference in normalization was necessary to preserve the depth-dependent structure of EMI

333   data, as ECa represents a bulk measurement where each reading is influenced by adjacent depths.

334   In contrast, NDVI measurements are independent and acquired at different time points, and thus

335   reflect temporal variations in vegetation dynamics.

336

337   In this study, a Self-Organizing Map (SOM), an unsupervised machine learning classification

338   technique, was used for clustering (Kohonen, 2013). SOM is a centroid-based clustering technique,

339   similar in some aspects to K-means clustering (Celebi et al., 2013). While K-means clustering

340   assigns each data point to a cluster based on the minimum distance to the cluster centroid in the

341   data space, SOM utilizes an artificial neural network to organize and visualize high-dimensional

342   data (Valentine and Kalnins, 2016). The key distinction lies in how SOM projects the data onto a

343   two-dimensional grid while preserving the topological relationships of the input data. Each data

344   vector in SOM is assigned to a numerical cluster, where the cluster centre is representative of all

345   the data points associated with it. These cluster centres, which have dimensions similar to the input

346   data vectors, adjust iteratively during the training process to better represent the underlying data

347   distribution. This approach allows SOM to effectively map complex data patterns while

348   maintaining the spatial relationships between clusters.

349

350   The Multi-Cluster Average Standard Deviation (MCASD) approach was used to determine the

351   optimal number of clusters for SOM. This method evaluates the stability of the cluster centres in

352   the dataspace over multiple clustering attempts as the number of clusters increases. This metric

353   assumes that an appropriate number of clusters for a dataset is any at which the cluster centres do

354   not vary significantly when the clustering algorithm is run multiple times. In this study, MCASD

355   analysis was tested with a maximum number of 20 clusters with 100 SOM clustering runs for each

356   number of clusters to calculate the MCASD stability metric. The number of clustering runs was

357   determined during preliminary testing, where it was observed that most datasets stabilized in terms

358   of variability between 70 and 80 iterations. To ensure consistency and reproducibility, we adopted

359   100 runs per cluster number. Upon completion of MCASD analysis, the highest number of clusters

360   with a low MCASD metric was selected, as this represents the maximum resolution of the spatial

361   variability that can be obtained through clustering (O'Leary et al., 2023). This clustering process

362   was performed in MATLAB v2023a (MathWorks, Natick, Massachusetts, USA).

363

364   **2.4 Statistical analysis**

365   To assess the differences between clusters derived from the three datasets, a one-way analysis of

366   variance (ANOVA) was conducted in SPSS (IBM, Chicago, IL, United States). ANOVA was used

367   to identify whether there were significant differences between clusters in terms of soil properties

368   or yield using a significance threshold of $p < 0.05$. Following the ANOVA, a Tukey's HSD

369   (Honestly Significant Difference) test was used as a post-hoc analysis to determine which of the

370   clusters were significantly different. In this step, the depth of the sandy layer, the texture of the

371   overlying layer, the texture of the layer below, and the yield data were used. Thus, this step is

372   complimentary to the previous cluster selection step with MCASD, which did not consider soil

373   and yield data. Clusters that did not exhibit significant differences were merged during a

374   reclassification step, refining the clustering results to ensure that each final cluster was distinct and

375   statistically meaningful, both in terms of the input datasets and in terms of soil properties and yield.

376   The latter was confirmed using two tailed t-tests between matching layers of adjacent soil classes

377   in the reclassified map.

378

3 Results and Discussion

3.1 ECa$_z$, NDVI, and yield maps

The ECa$_z$, NDVI, and yield maps highlight unique aspects of field heterogeneity and offer insights into subsurface soil properties, above-ground crop performance, and their combined effects on productivity. In the following, these input datasets for management zone delineation are briefly introduced.

3.1.1 EMI maps

Nine ECa maps with 3 m resolution were obtained from the interpolation of the nine coil configurations recorded during the EMI measurements. The results for one coil configuration (HCP 050 cm) are exemplary shown in (Figure 3) before and after normalization. The study area was measured under varying conditions in terms of soil temperature, soil moisture, and effect of agricultural management. This resulted in differences of average ECa and spatial patterns (Figure 3a). Although it is well known that temperature affects measured ECa (Pedrera-Parrilla et al., 2016; Vogel et al., 2019), it was not possible to perform a comprehensive temperature correction in this study due to the lack of sufficient soil temperature data. Moreover, it has been shown that temperature correction has limitations compared to normalization methods when the dataset is composed of various depths of investigation and is affected by multiple agricultural management practices (Brogi et al., 2019; Rudolph et al., 2015). Thus, Z-score normalization was applied for each measurement campaign to reduce the differences between data measured on different days. Figure 3b shows the normalized EMI map for the same coil configuration as shown in (Figure 3a). The normalization successfully harmonized the data, minimizing the influence of varying soil moisture and temperature during acquisition, resulting in more consistent spatial patterns that

402 better represent subsurface soil properties. However, some localized artefacts in the normalized

403 maps still persist. For example, areas near the field boundaries or experimental patches exhibit

404 subtle inconsistencies that may be influenced by edge effects or localized disturbances. Despite

405 these minor limitations, the normalized ECa maps provide a robust foundation for further analysis

406 and management zone delineation.

407

408
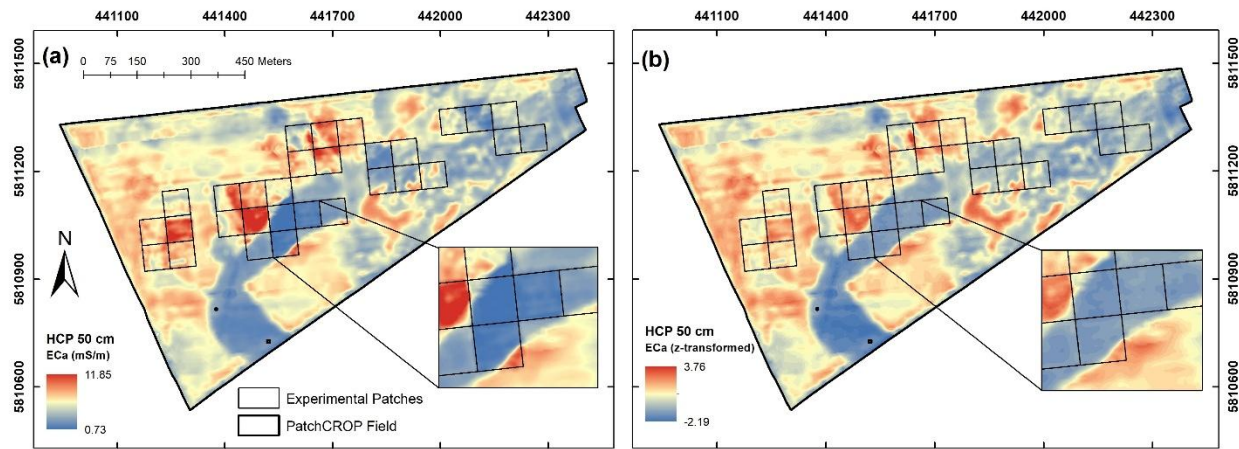
409 Figure 3. Comparison of apparent electrical conductivity (ECa) maps before and after z-score

410 normalization for the HCP 50 cm configuration with **(a)** the non-normalized ECa map, where the

411 zoomed-in section highlights the influence of varying environmental conditions such as soil

412 moisture and temperature leading to inconsistent patterns and **(b)** the z-score normalized ECa map,

413 which minimizes the influence of these external factors.

414

415 Figure 4 shows the nine normalized ECa_z maps for the VCP and HCP configurations. These maps

416 display heterogeneous patterns of ECa, primarily attributed to variations in soil characteristics in

417 space and with depth. A prominent feature is the elongated channel extending from the northeast

418 to the southwest of the field, which represents areas with lower ECa_z values. This feature is

419   associated with sandy soils that generally hold less water and nutrients, indicating a coarse-

420   textured zone with lower electrical conductivity. In contrast, the northwest and southeast regions

421   of the field exhibit medium to high ECa_z values, which may reflect areas of higher moisture content

422   and finer soil particles, such as loamy textures. Additionally, in the northeastern part of the field,

423   a more heterogeneous area with short-scale variations can be observed where the ECa_z values vary

424   considerably between the nine maps. For the shallow VCP configurations, this area shows low

425   ECa_z values, which are indicative of sandy soils or dry conditions near the surface. For the deeper

426   HCP configurations, this same area shows higher ECa_z values, suggesting an increase in soil

427   moisture or finer soil texture at greater depths. This pattern highlights the layered soil

428   heterogeneity in this region, with subsurface properties differing significantly from the surface.

429   Overall, the EMI data reveal a high degree of spatial variability and provide valuable insights into

430   subsurface soil variability, which is critical for precision agricultural management.

431

432
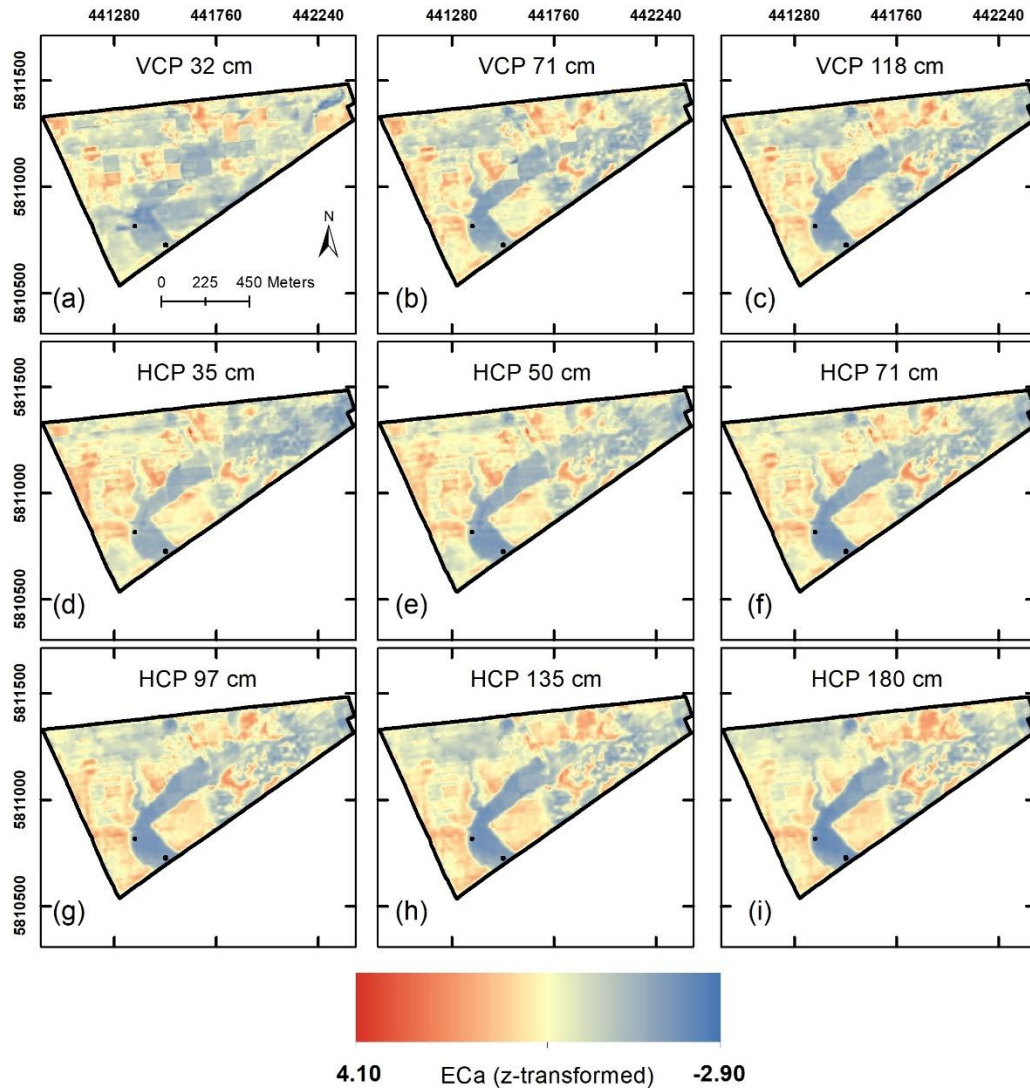
Figure 4. Normalized apparent electrical conductivity (ECaz) maps derived from electromagnetic

induction (EMI) measurements using multiple coil separations in vertical coplanar (VCP) and

horizontal coplanar (HCP) configurations (see Table *1* for more details). These maps highlight the

spatial variability of subsurface soil properties, with higher ECaz values (red) indicating areas of

higher moisture retention or finer soil textures, and lower ECaz values (blue) corresponding to

sandy soils with lower conductivity.

439

440

3.1.2 NDVI maps

All available PlanetScope satellite images for the growing season 2019 (winter rye) were visually

evaluated to assess their usability. Before April 2019, no meaningful patterns in NDVI were

observed due to the relatively short height (10 to 20 cm) and low biomass of winter rye and the

lack of water- or nutrient-induced stress in this early growth stage. Moreover, images from July

2019 were excluded from the analysis as the crop had reached maturity, and no further growth or

development was evident. By this time, the physiological activity of the plants had ceased, and

harvesting was completed on 04/08/2019.

After this initial analysis, seven NDVI images spanning the period between April and June, hence

from flowering to maturity, were selected for further analysis (Figure 5). The descriptive statistics

of the NDVI data are given in Table 2 and show a high degree of temporal variation. Following

crop development during the growing season, the mean NDVI peaked on 30 April 2019 (221 days

after sowing). Afterwards, NDVI values gradually declined as the crop approached maturity, which

is consistent with physiological changes during growth of winter rye (Hatfield and Prueger, 2010).

Figure 5 illustrates the temporal development of the spatial variation of NDVI, highlighting the

spatial heterogeneity of crop performance within the field (especially Figure 5d-g) where areas of

lower NDVI are associated with poorer crop performance and areas of higher NDVI indicate

healthier crops. Generally, the key patterns in crop performance are in good agreement with the

patterns observed in the EMI maps. Areas with persistently low NDVI values generally correspond

to areas with low ECa_z, and areas with high NDVI values mostly correspond to areas with high

ECa_z. However, differences between patterns in NDVI and EMI can also be found. This is expected

given that the dynamic changes in crop vigour and vegetation health shown by NDVI are not solely

related to subsurface soil conditions captured by EMI. For example, specific areas with low NDVI values were observed in regions of medium to high ECa_z, possibly reflecting localized crop stress due to non-soil-related factors such as disease, waterlogging, or nutrient imbalances.

Table 2. Summary of remotely sensed NDVI imagery and corresponding dates after sowing.

Date of acquisition	Days after sowing	Mean NDVI	Max NDVI	Min NDVI
05 April 2019	196	0.67	0.78	0.42
16 April 2019	207	0.72	0.85	0.46
30 April 2019	221	0.76	0.88	0.38
11 May 2019	232	0.61	0.71	0.34
30 May 2019	251	0.58	0.66	0.41
12 June 2019	263	0.49	0.65	0.31
24 June 2019	276	0.49	0.71	0.30
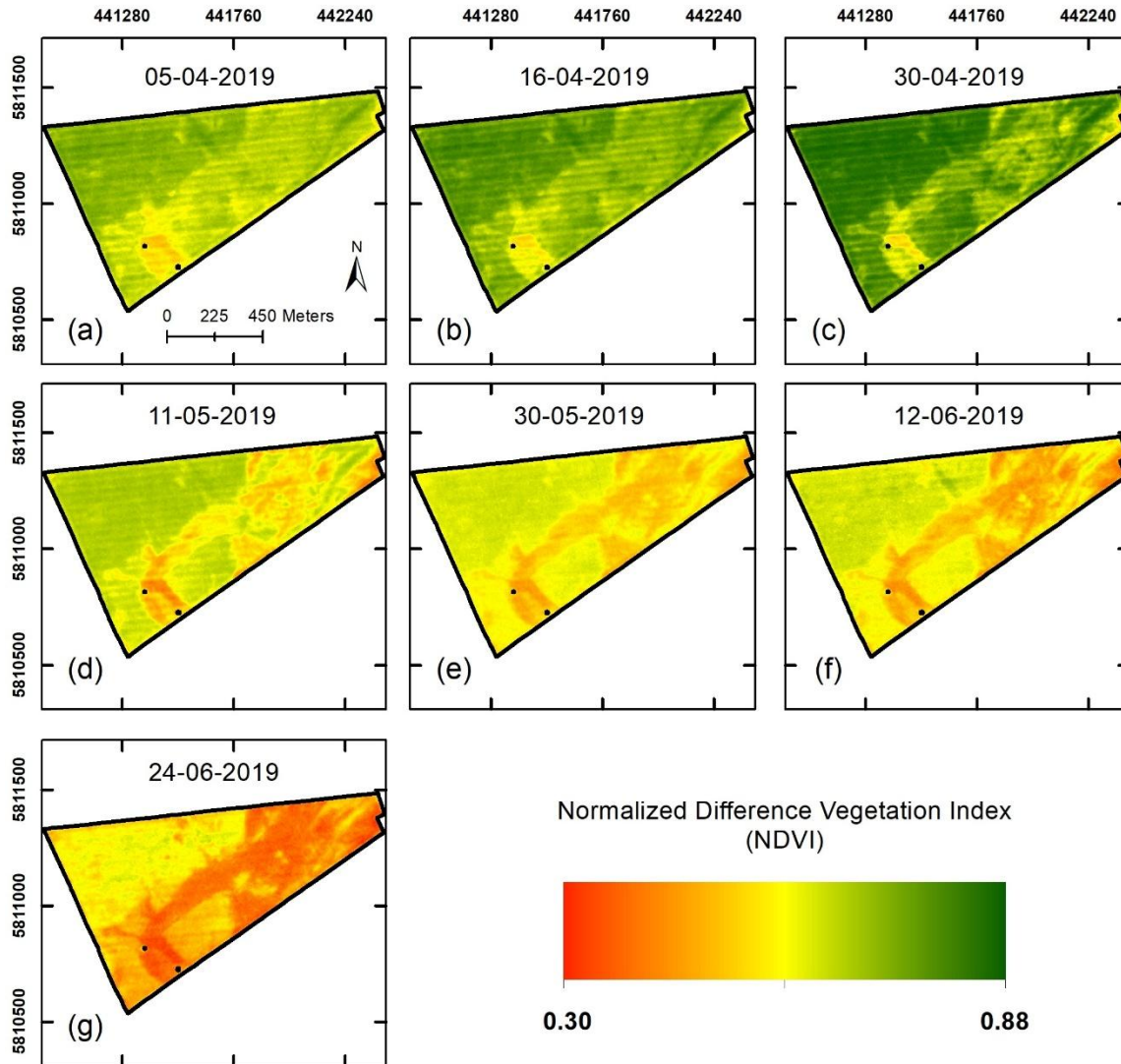
Figure 5. Seven NDVI maps derived from PlanetScope satellite imagery representing the temporal variability in vegetation development during the 2019 growing season. The images, dated from 05-04-2019 to 24-06-2019, capture critical crop growth stages, including flowering and maturity.

3.1.3 Yield maps

Figure 6 presents nine years (2011–2019) of yield maps interpolated at a 10 m resolution to represent spatial variability across the field. The maps illustrate distinct patterns of high and low productivity areas. Yield variability is consistent across multiple years, although variations in

480   measured yield can be observed between years. The years 2012 and 2013 show lower quality yield

481   data due to incomplete datasets (Donat et al., 2022) caused by equipment issues and environmental

482   challenges during data collection. Despite these limitations, they were retained for spatial context

483   as they still exhibited consistent patterns with other years, and the maps successfully captured the

484   general spatial yield trends and heterogeneity of the field. These years were not weighted

485   differently during validation, and the potential influence of this lack of weighting was mitigated

486   by evaluating multi-year trends and conducting year-by-year comparisons (see Section 3.4). The

487   high and low yield zones align with known intrinsic field characteristics, such as soil texture,

488   moisture retention, and nutrient availability (Grahmann et al., 2024). These yield patterns will

489   serve as validation for comparing the management zones derived from EMI and NDVI data, as

490   both datasets aim to explain the variability in productivity.

491

492
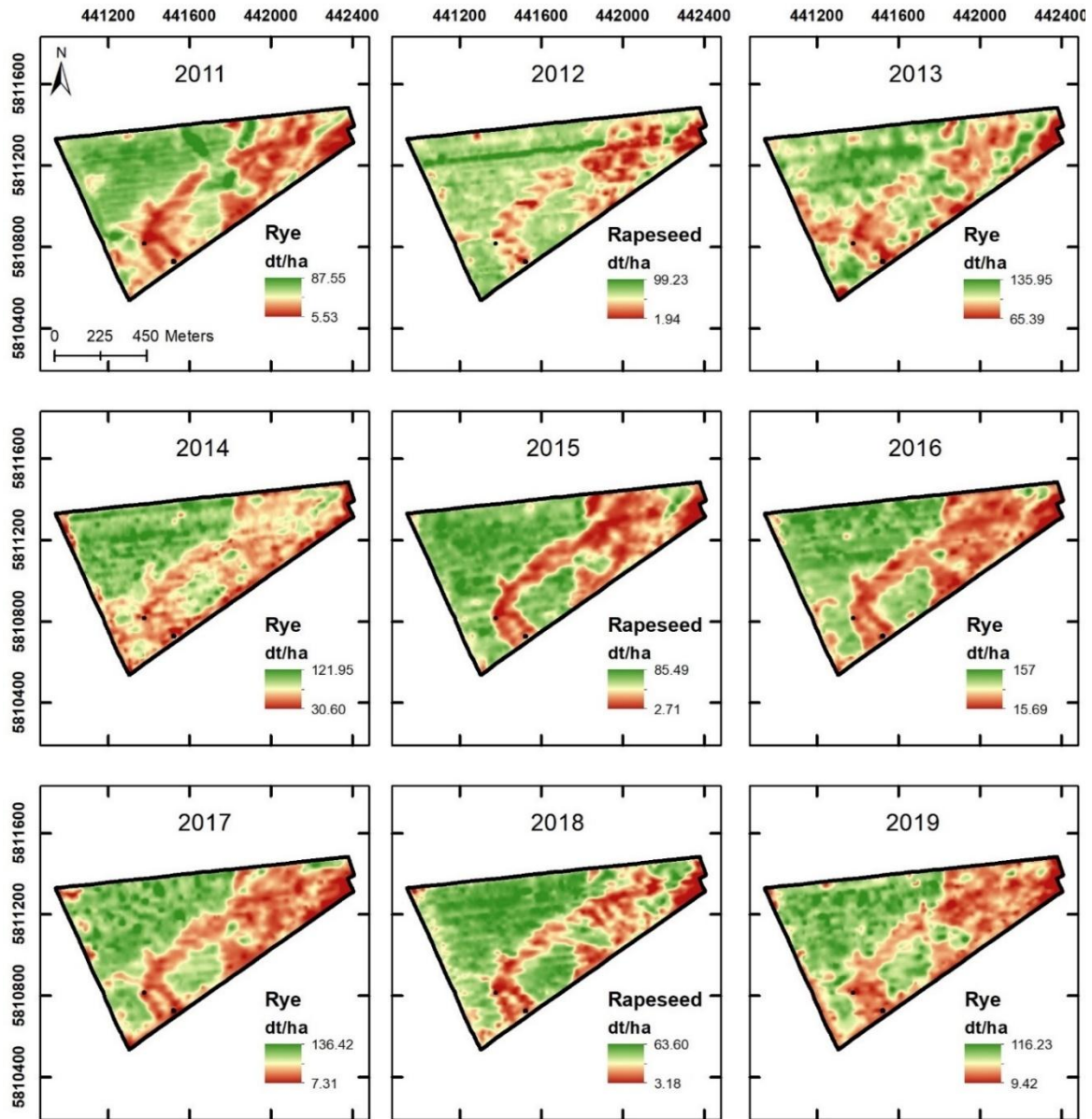
493 Figure 6: Nine interpolated yield maps (2011–2019) for the patchCROP field showing spatial

494 variability of crop yield at a 10 m resolution. The maps illustrate yield distributions for winter rye

495 (2011, 2013, 2014, 2016, 2017, 2019) and rapeseed (2012, 2015, 2018). High-yield areas (green)

496 and low-yield areas (red) reflect the inherent field heterogeneity. Variability is observed both

497 within and across years, influenced by crop type, management practices, and environmental

498 conditions. The yield range for each year is provided in decitonnes per hectare (dt/ha).

3.2 Clustering of EMI and NDVI

The MCASD analysis for the three datasets provided a robust method to determine the optimal number of clusters (Figure 7). The analysis suggested a maximum of five clusters for the EMI data (Figure 7b). These clusters reflect differences in subsurface properties such as soil texture, moisture, and compaction. Cluster 1 corresponds to areas with the highest ECa_z values, which gradually decrease with each subsequent cluster. Cluster 5 represents the lowest ECa_z values. For NDVI (Figure 7e), a maximum of four clusters was selected. While a five-cluster solution was initially identified as viable for NDVI, increasing the number of clusters beyond four did not significantly reduce variability. This made the four-cluster solution more practical and efficient for representing spatial variability in the NDVI data. Cluster 1 identifies areas with relatively high NDVI values, indicative of healthy, dense vegetation and higher crop performance. NDVI values progressively decrease with higher cluster numbers, with cluster 4 showing the lowest values, representing stressed or less productive areas. The combined EMI and NDVI dataset resulted in four clusters (Figure 7h). Visual inspection suggests that both the EMI- and NDVI-based patterns are preserved in the combined dataset, likely due to the min-max scaling applied to standardize each dataset before MCASD analysis (see Appendix A). Clusters 1 and 2 represent areas with high values for both ECa_z and NDVI, while cluster 4 identifies zones with low values for both variables, integrating both above-ground and subsurface variability effectively.

518
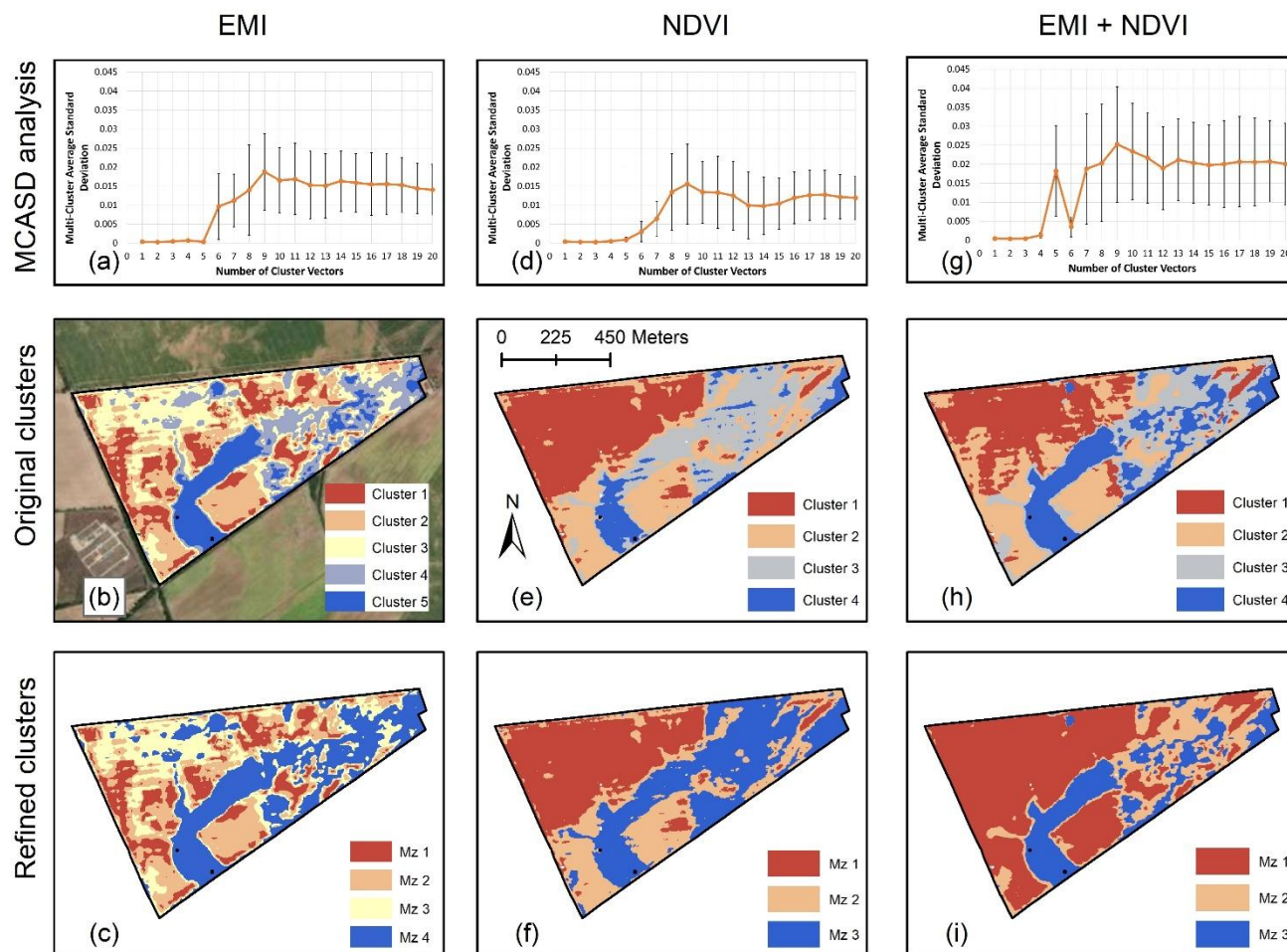
519 Figure 7. Clustering results for the PatchCROP experimental site. **(a)** MCASD analysis showing

520 appropriate cluster numbers for EMI data. **(b)** Spatial distribution of original EMI clusters (ESRI,

521 2020). **(c)** Spatial distribution of refined EMI clusters after post-hoc analysis. **(d)** MCASD analysis

522 for NDVI data. **(e)** Spatial distribution of original NDVI clusters. **(f)** Spatial distribution of refined

523 NDVI clusters after post-hoc analysis. **(g)** MCASD analysis for the combined (EMI + NDVI)

524 dataset. **(h)** Spatial distribution of the original clusters based on the EMI and NDVI data. **(i)** Spatial

525 distribution of the refined clusters for the combined dataset after post-hoc analysis.

526

527

528

3.3 Post-hoc analysis

530 Starting from the optimal number of clusters identified with MCASD, a post-hoc analysis based

531 on the nine available yield maps and the point-scale soil samples was conducted. The aim was to

532 verify that the cluster are not only statistically separated in terms of the input data (i.e., EMI, NDVI

533 or a combination of EMI and NDVI), but also in terms of yield and soil characteristics (i.e., texture

534 of the first and second layers, depth to the second layer). For the EMI-based clusters, 18 soil

535 sampling locations were within Cluster 4 and only four of these had an EOS layer within 100 cm

536 depth. The other 14 locations had EOS layer below the sampling depth of 100 cm and thus no

537 textural values for the lower layer. Thus, the EOS layer depth of Cluster 4 was assumed to be below

538 100 cm, and the texture of the lower layer was excluded from further analysis to have a more

539 consistent characterization of the prevailing soil characteristics.

540

541 Post-hoc analysis indicated that not all clusters were significantly different from each other, either

542 in terms of yield or soil characteristics. Based on the results of the post-hoc analysis, clusters were

543 either left separated when yield or soil characteristics were statistically different ($p < 0.05$) or

544 grouped together when no statistical separation was identified. For example, Clusters 1, 2, and 3

545 of the EMI-based classification had at least one significant difference in texture, EOS layer, or

546 yield. On the contrary, cluster 4 and 5 did not show statistically significant differences for any of

547 the investigated properties. Thus, Cluster 4 and 5 were merged together and the resulting EMI-

548 based cluster map had four clusters with statistically significant separation of input data (i.e., EMI),

549 yield, and soil characteristics. A more detailed breakdown of this post-hoc analysis and the

550 resulting merging decisions is provided in Appendix B.

551

After this post-hoc analysis, the resulting refined maps (Figure 7c, f and i) now have clusters that are statistically separated in terms of the input dataset (i.e., EMI and NDVI) but also in terms of the target variables, which are yield and soil characteristics. Therefore, they are referred to as management zones instead of clusters from this point onwards. These management zone maps appear to be a simplification of the original clustered maps (Figure 7b, e and h), but they now provide a more holistic understanding of the field by integrating below-ground (EMI) and above-ground (NDVI) information with yield and soil data.

559

3.4 Assessment of management zones derived from different datasets

For each management zone of the maps derived from EMI, NDVI, and a combination of EMI-NDVI, Table 3 shows the average yield between 2011 and 2019 and average soil characteristics, specifically the depth of the soil texture transition (EOS) and the textural fractions (percentages of sand, silt, and clay) of two layers up to 100 cm depth. The average yields of Table 3 vary considerably between different years and follow a general trend of decreasing yields with increasing cluster number. Thus, yields decrease with decreasing ECa_z and NDVI.

567

568 Table 3. Average values of yield (dt/ha) and soil properties for the management zones (MZs)

569 derived from EMI, NDVI, and a combination of EMI and NDVI.

			EMI				NDVI			EMI-NDVI		
		MZs	**1**	**2**	**3**	**4**	**1**	**2**	**3**	**1**	**2**	**3**
Yield		**2011**	49.5	44.7	46.5	31.7	55.9	41.1	27.5	50.7	33.1	25.7
		2012	53.4	53.1	52.6	38	57.9	52.2	34.4	56.2	41.2	32.6
		2013	106.3	105.6	106.5	98.1	111.1	104.9	94.49	108.8	99.1	93.4
		2014	86.4	83.9	86.3	72.5	95.3	78.5	69.0	89.3	72.5	67.8
		2015	55.1	53.7	51.0	28.5	62.9	50.1	22.2	59.1	31.1	20.5
		2016	94.0	93.1	90.2	62.3	108.5	85.2	53.4	101	61.4	53.0
		2017	78.7	76.0	73.7	47.9	89.4	69.4	41.0	83.3	48.5	39.5
		2018	40.3	39.6	38.8	26.9	44.8	37.6	23.7	42.6	29.0	21.9
		2019	71.0	69.1	67.2	48.1	80.2	62.5	43.1	74.6	47.7	42.2
Soil characteristics	**Layer 1 (above EOS)**	**Sand %**	68.2	72.4	78.1	86.2	68.6	79.5	87.2	69.8	88.4	85.2
		Silt %	23.3	20.0	16.1	9.6	23.0	15.2	8.9	22.2	8.1	10.4
		Clay %	8.5	6.9	5.7	4.1	8.0	5.2	3.8	7.7	3.4	4.3
		Depth (cm)	54.0	66.9	73.1	100	62.7	71.0	87.4	63.8	77.0	100
	Layer 2 (below EOS)	**Sand %**	58.3	58.0	60.6	NA	58.1	57.8	66.1	58.1	64.9	NA
		Silt %	23.0	23.2	21.9	NA	23.1	23.1	19.3	23.1	19.9	NA
		Clay %	18.6	18.7	17.5	NA	18.7	19.0	14.5	18.8	15.1	NA

570

571 Figure 8 shows the variation in rye yield (dt/ha) for the management zones derived from different

572 data sources for the year 2019, which is considered representative for most previous years while

573 also allowing a direct comparison with the NDVI data for the 2019 growing season. For the EMI-

574 based management zones (Figure 8a), the yield distributions for the zones 1-3 are relatively similar,

575 with overlapping interquartile ranges and medians. This indicates that the EMI-based management

576 zones are more reflective of subsurface soil properties than yield variability for this particular field.

577   However, zone 4 showed significantly lower yields, corresponding to sandy soils with poor

578   moisture retention (see Table 3). The NDVI-based management zones (Figure 8b) demonstrate

579   stronger differentiation in yield distribution and a more consistent decline in yield between zones,

580   reflecting the ability of NDVI to capture above-ground vegetation vigour and crop health. In

581   particular, zone 2 reflects an intermediate yield zone between zone 1 and 3, showcasing the ability

582   of NDVI to differentiate changes in crop performance. The management zones derived from

583   combining EMI and NDVI (Figure 8c) offer narrower interquartile ranges, particularly in zone 2,

584   compared to NDVI-based management zones. This indicates that the integration of EMI and NDVI

585   provides a more consistent and stable representation of yield variability, combining subsurface soil

586   properties with above-ground dynamics. Although NDVI alone offers slightly more pronounced

587   yield differentiation, the combined dataset balances both subsurface and vegetation-related factors

588   effectively, making it a robust approach for management zone delineation. Similar boxplots for

589   additional years are provided in Appendix C.

590

591
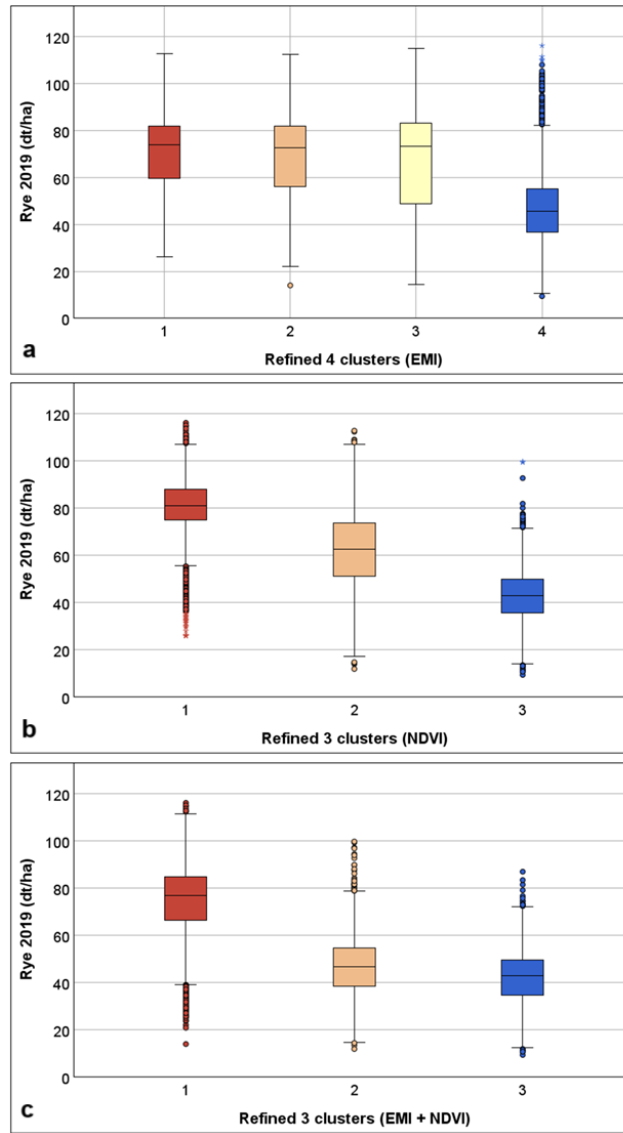
592   Figure 8. Boxplots illustrating rye yield (dt/ha) for 2019 across management zones (MZs)

593   derived from **(a)** EMI, **(b)** NDVI, and **(c)** a combination of EMI and NDVI datasets.

594

595   The refined management zones can be associated with a typical soil profile based on the average

596   soil characteristics (Figure 9). The soil profiles show the textural properties of the first two soil

597   layers and the depth of the interface between these layers (EOS) up to a depth of 100 cm. In some

598   profiles, the EOS layer reaches 100 cm, and thus the textural properties of the second layer are not

599 available. In case of the EMI-based zones (Figure 9a-b), zone 1 is characterized by generally higher

600 ECa_z values, and identifies areas with a substantial average clay content, especially in the second

601 soil layer (18.6%). Moreover, the sandier top layer is rather shallow and reaches depth of around

602 54 cm. Moving from zone 1 to zone 4, ECa_z generally decreases. At the same time, the depth of

603 the top layer (EOS) becomes deeper while the clay and silt content of the soil decreases and the

604 sand content increases. In zone 4, the average clay content up to 100 cm is 4.1%, while the sand

605 content is 86.2%. In the case of the NDVI-based management zones (Figure 9c-d), the three zones

606 appear to be more indicative of crop development, which results in typical soil profiles with

607 differences that seem less pronounced compared to the case of EMI-based zonation. In this case,

608 NDVI is generally higher in Cluster 1 and lowest in Cluster 3. The change in soil characteristics

609 between zones follows a similar trend compared to that of EMI-based zones. The depth of the

610 interface between soil layer 1 and 2 increases from 62.7 to 87.4 cm from zone 1 to 3, while the

611 sand content of both layers also increases (from 68.6 to 87.2 % and 58.1 to 66.1 %, respectively).

612 The management zones derived from the combined EMI-NDVI dataset (Figure 9e-f) have typical

613 soil profiles that are similar to those based on NDVI. Also, the sand, silt, and clay content of the

614 first soil layer appear to be rather similar. However, the range of the depth of the interface between

615 soil layer 1 and 2 is higher for the EMI-NDVI clustered map (63.8 to 100 cm) compared to that of

616 NDVI-based profiles (62.7 to 87.4 cm). At the same time, the difference in texture between the

617 second soil layer of Clusters 1 and 2 is stronger in the profiles based on a combination of EMI and

618 NDVI data (see Table 3). These two factors show that the management zones from EMI and NDVI

619 have a relatively high variation between soils of different management zones, which is an

620 improvement compared to the case of the NDVI-based management zones.

621
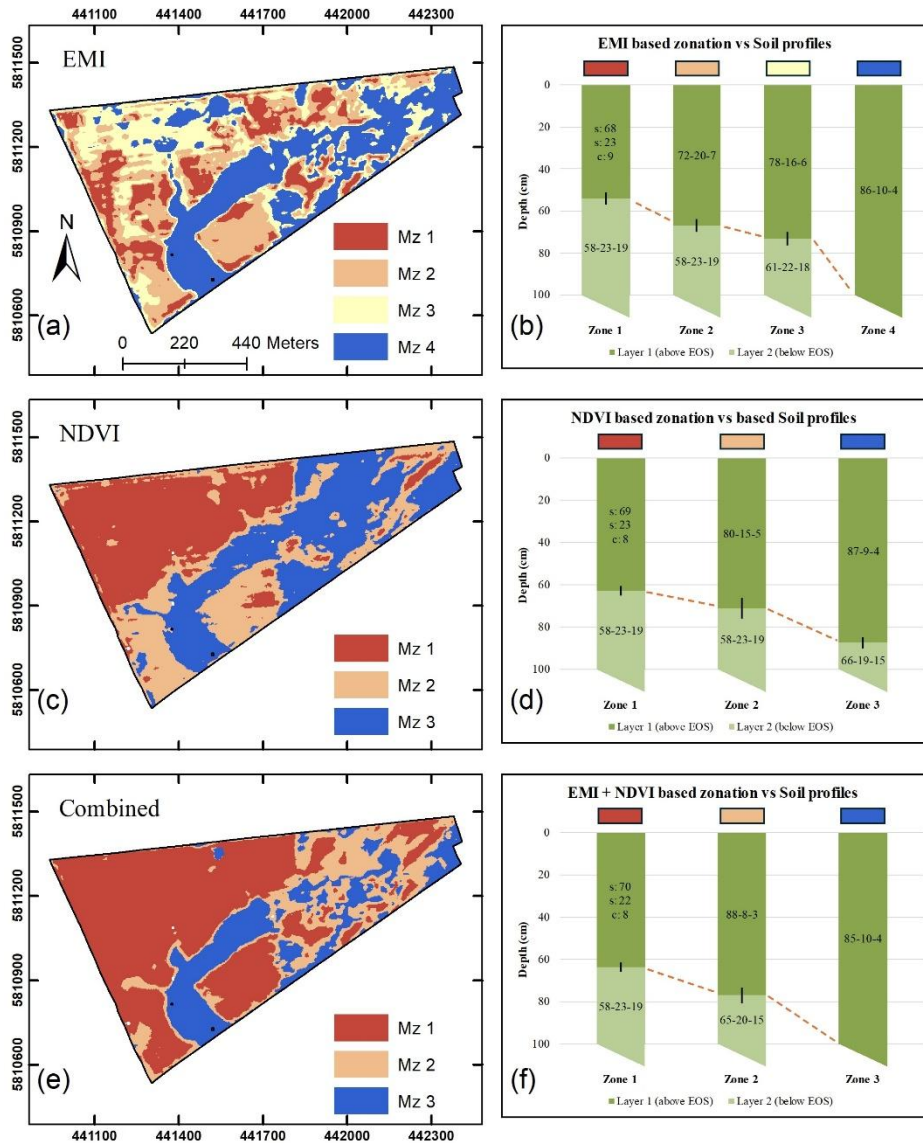
Figure 9. Final management zone maps derived from **(a)** EMI, **(c)** NDVI, and **(e)** a combination

of EMI and NDVI datasets. Each zone represents areas with similar subsurface and/or above-

ground characteristics. **(b, d, f)** Corresponding soil profiles for each management zone, detailing

soil texture (sand-silt-clay %), dotted lines between zones indicate depth of textural change (Layer

1: above EOS; Layer 2: below EOS) and error bar represents the standard error.

627

628   In a final step, statistical validation of the management zones was conducted using pairwise t-tests

629   to evaluate the degree of significant differences in yield and soil properties across consecutive

630   zones. The results are summarized in Table 4. A pairwise t-test for neighbouring zones derived

631   from EMI indicated that the yield of 2012, 2013, and 2016 was not significantly different between

632   zone 1 and zone 2 (p = 0.603, 0.060, 0.253) while the yield of 2012 was not significantly different

633   between zone 2 and 3 (p = 0.209). All other pairwise comparisons indicated significant differences

634   in mean yield. The textural composition of layer 1 was significantly different between all EMI-

635   derived zones. On the contrary, the depth of top layer was not significantly different between zone

636   2 and 3 (p = 0.167). In addition, the composition of soil layer 2 was not significantly different

637   between zone 1 and 2 (p of 0.498 for sand, 0.636 for silt, and 0.805 for clay).

638

639   The pairwise t-tests between neighbouring zones based on NDVI indicated that differences in yield

640   among all investigated years were statistically significant. On the contrary, both the depth of the

641   top layer and the composition of soil layer 2 were not significantly different between zone 1 and 2

642   (p of 0.147 for depth, 0.558 for sand, 0.986 for silt, and 0.627 for clay). These results show that

643   EMI-based zones subdivided the area in one additional class and provided a more comprehensive

644   representation of soil properties up to 100 cm compared to the NDVI-based zones for the

645   investigated field. At the same time, the NDVI-based zones offered a better representation of yield

646   from 2011 to 2019.

647

648   The pairwise t-test between neighbouring zones based on the combined EMI-NDVI dataset

649   showed that the three zones were significantly different for both yield and soil characteristics. This

650   indicates that integrating EMI and NDVI datasets allows for the delineation of zones that are robust

651   in representing both yield variability and soil heterogeneity. Moreover, a visual inspection of the

652   management zone maps (Figure 9) shows that both maps based solely on EMI or NDVI are

653   affected by West-East oriented patterns due to measurement direction for EMI and tractor lines in

654   NDVI. These features are not present in the management zone map that integrates EMI and NDVI,

655   suggesting that it also provides a representation of the field that is less affected by external factors.

656   These results underscore the added value of integrating complementary datasets to capture the full

657   spectrum of variability within the field, supporting more informed and effective precision

658   agriculture practices.

659

660 Table 4. Results of the pairwise t-tests for yield and soil properties between management zones

661 derived from EMI, NDVI, and EMI-NDVI. Bold font indicates significant differences.

			EMI			NDVI		EMI - NDVI	
		Cluster	1vs2	2vs3	3vs4	1vs2	2vs3	1vs2	2vs3
Yield		2011	**< 0.001**	**< 0.001**	**< 0.001**	**< 0.001**	**< 0.001**	**< 0.001**	**< 0.001**
		2012	0.603	0.209	**< 0.001**	**< 0.001**	**< 0.001**	**< 0.001**	**< 0.001**
		2013	0.060	**0.008**	**< 0.001**	**< 0.001**	**< 0.001**	**< 0.001**	**< 0.001**
		2014	**< 0.001**	**< 0.001**	**< 0.001**	**< 0.001**	**< 0.001**	**< 0.001**	**< 0.001**
		2015	**0.007**	**< 0.001**	**< 0.001**	**< 0.001**	**< 0.001**	**< 0.001**	**< 0.001**
		2016	0.253	**< 0.001**	**< 0.001**	**< 0.001**	**< 0.001**	**< 0.001**	**< 0.001**
		2017	**< 0.001**	**0.002**	**< 0.001**	**< 0.001**	**< 0.001**	**< 0.001**	**< 0.001**
		2018	**0.039**	**0.007**	**< 0.001**	**< 0.001**	**< 0.001**	**< 0.001**	**< 0.001**
		2019	**0.002**	**0.003**	**< 0.001**	**< 0.001**	**< 0.001**	**< 0.001**	**< 0.001**
Soil	Layer 1 (above EOS)	Sand %	**< 0.001**	**0.001**	**< 0.001**	**< 0.001**	**< 0.001**	**< 0.001**	**< 0.001**
		Silt %	**< 0.001**	**0.006**	**< 0.001**	**< 0.001**	**< 0.001**	**< 0.001**	**< 0.001**
		Clay %	**< 0.001**	**0.014**	**< 0.001**	**< 0.001**	**< 0.001**	**< 0.001**	**< 0.001**
		Depth (cm)	**0.004**	0.167	**NA**	0.147	**0.004**	**0.002**	**NA**
	Layer 2 (below EOS)	Sand %	0.498	**0.010**	NA	0.558	**< 0.001**	**< 0.001**	NA
		Silt %	0.636	**0.009**	NA	0.986	**0.004**	**0.003**	NA
		Clay %	0.805	0.056	NA	0.627	**< 0.001**	**< 0.001**	NA

662

663 **3.5 Limitations and perspectives for future work**

664 This study successfully demonstrated the integration of EMI and NDVI datasets for the delineation

665 of management zones, but some limitations are still present and should be addressed in future

666 research. The EMI data were collected during different campaigns under varying environmental

667 conditions (e.g., soil temperature and moisture) and thus required z-score normalization to

668 minimize variability. While effective in this study, this approach may not fully account for certain

669   external factors such as the impact of different management practices in different parts of the field.

670   Similarly, the NDVI dataset was limited to the 2019 growing season as a) PlanetScope imagery

671   became accessible for this region only in 2019 and b) the subdivision of the field in differently

672   cultivated patches from 2020 prevented the use of later satellite products. Nonetheless, the choice

673   of PlanetScope imagery (3 m resolution) enabled to capture detailed within-field variability in

674   NDVI, which was particularly important in this study area due to the spatial heterogeneity

675   introduced by soil variation. If coarser-resolution imagery such as Sentinel-2 (10 m) were used

676   instead, smaller-scale patterns in crop development or soil-related variation would have been less

677   detectable due to spatial averaging. This could have reduced the effectiveness of the SOM

678   clustering in identifying distinct management zones. However, for more homogeneous or large-

679   scale fields, Sentinel-2 data could be a practical and freely accessible alternative (Kaya et al.,

680   2025). Another limitation of this study is that the 2019 dataset was considered to be representative

681   of the investigated area. However, a single season of NDVI data may not fully capture interannual

682   variability driven by climatic conditions or crop management practices (Scudiero et al., 2018).

683   Incorporating NDVI data from multiple years in future studies could enable a more comprehensive

684   analysis of temporal dynamics and their impact on management zone delineation to capture yield

685   and soil variability.

686

687   A further limitation of the study design was the distribution of soil sampling locations. Although

688   the 160 sampling points provided valuable insights, leveraging EMI-based maps to guide targeted

689   soil sampling could improve spatial representativeness. Additionally, while EMI in this study had

690   a depth of investigation of up to 270 cm, soil sampling was limited to 100 cm depth, potentially

691   missing soil heterogeneity that can affect crops.

692

Regarding data process, min-max scaling was a suitable method in this study due to the relatively smooth and filtered input data, both for EMI and NDVI. However, this scaling approach is known to be sensitive to outliers and data range extremes (Pedregosa et al., 2011). For datasets with greater variability or different preprocessing methods, alternative scaling approaches such as standardization or robust scaling could be more appropriate (de Amorim et al., 2023). Another factor was the proper application of data normalization prior to clustering, which was essential for obtaining meaningful results in this study (see Appendix A). Future studies should assess the impact of different scaling and normalization strategies on clustering outcomes, especially in settings with noisier or unfiltered sensor data.

702

In this study, clustering relied on a combination of Multi-Cluster Average Standard Deviation (MCASD) to determine the optimal number of clusters and self-organized maps (SOM). While cluster variability was addressed using the Multi-Cluster Average Standard Deviation (MCASD) across 100 SOM runs to a large extent, future studies may benefit from incorporating additional stability metrics such as the Adjusted Rand Index (ARI) or cluster overlap measures to better assess classification consistency. The availability of yield and soil data supported the refinement of SOM-based clusters, enabling the merging of groups that were not agronomically distinct. These datasets helped to ensure that the final management zones were both data-driven and interpretable. However, in scenarios where such ground-truth data are limited or unavailable, the initial clusters may still offer useful insights, albeit with greater uncertainty in their agronomic interpretation. Thus, the presented post-hoc validation step added confidence in the results, but is not strictly required.

715

716 The SOM algorithm and the statistical methods used in this study (ANOVA, Tukey's HSD, and t-

717 tests) do not explicitly account for spatial autocorrelation, which is inherently present in the

718 interpolated geospatial datasets used here. This may influence statistical outcomes or lead to less

719 spatially coherent clusters in some cases. For instance, kriging interpolation introduces a spatial

720 structure that may challenge the assumption of independence underlying post-hoc statistical tests.

721 However, the use of multi-year yield trends and high-resolution soil data helped reduce uncertainty

722 in post-hoc validation. Future studies may benefit from incorporating spatially explicit methods,

723 such as spatially constrained clustering, variogram-based diagnostics, or spatial ANOVA, to better

724 account for spatial dependence during both classification and validation stages. In addition to these

725 methodological considerations, future studies should focus on improving the temporal consistency

726 of data collection and increasing the density and depth of soil sampling. The quantification of

727 uncertainty in management zone delineation could be also investigated, for example through

728 ensemble clustering or by incorporating uncertainty from spatial inputs such as EMI interpolation.

729 Finally, long-term monitoring using datasets from multiple years could provide insights into the

730 temporal stability of management zones and their relationship with yield.

731

732 The detailed management zone maps complemented with soil characterization obtained in this

733 study should in a next step be integrated into agroecosystem models. This well enable to simulate

734 and predict the impact of different management strategies under future environmental and climatic

735 conditions, and thus help to optimize irrigation, fertilization, and other field management practices,

736 further supporting decision-making for sustainable and resource-efficient agriculture.

737

4 Conclusions

This study integrated proximal soil sensing (EMI) and remote sensing (NDVI) data to delineate high-resolution management zones in a 70 ha agricultural field. Self-Organizing Maps (SOM), an advanced unsupervised machine learning technique, were combined with statistical validation methods to identify spatial areas with similar above- and below-ground properties. Historical yield maps and detailed soil information up to a depth of 100 cm were used to refine and validate the clustering results, ensuring both their accuracy and practical applicability.

To address the variability introduced by environmental conditions during data collection, EMI measurements from multiple campaigns were standardized using z-score normalization, ensuring consistent input for further analysis of the investigated field. Similarly, NDVI data from the 2019 growing season were selected as they represented an uninterrupted crop cycle prior to the subdivision of the investigated field in multiple patches. Before clustering, data was appropriately normalized. The Multi-Cluster Average Standard Deviation (MCASD) method was applied to determine the optimal number of clusters for different datasets. The optimal number of clusters was determined to be five using the EMI data, four for the NDVI data, and four for the combination of EMI and NDVI datasets. However, statistical validation through Tukey's post-hoc analysis using independent yield maps and soil samples reduced the clusters number to 4, 3, and 3, respectively. This ensured that the clusters were not only computationally distinct with respect to the input data, but also significantly different in terms of soil characteristics and yield data, thereby increasing their practical relevance in precision agriculture.

760 Results showed that EMI-based management zones provided a better representation of subsurface

761 properties, particularly soil texture and the depth at which textural changes occur, which underlines

762 the utility of EMI for guiding soil management practices. In comparison, NDVI-based

763 management zones aligned more closely with topsoil characteristics and yield maps, effectively

764 capturing above-ground variability. In general, the integration of EMI and NDVI datasets provided

765 a more comprehensive representation of the spatial variability of both soil characteristics and yield,

766 resulting in management zones that linked both subsurface soil conditions and above-ground

767 vegetation performance. These combined zones effectively explained productivity patterns by

768 bridging the gap between soil properties and crop health.

769

770 The product of this study is a high-resolution management zonation map which would provide a

771 significant added value in precision and sustainable agriculture. Moreover, it can help in setting-

772 up of agroecosystem models for the simulation of crop performance and yield and in guiding future

773 soil sampling campaigns. Finally, the workflow proposed in this study can provide a robust

774 blueprint for unsupervised clustering of proximal soils sensing and remote sensing data in

775 agriculture, and future studies should explore the scalability of this methodology in different

776 climatic conditions or other crop systems, as well as investigate additional data sources to further

777 enhance the representation of within-field heterogeneity in soil and crops.

778 **Appendix A: Influence of data normalization**

779 Figure A1 shows a visual comparison of management zone delineation using different

780 normalization approaches. These are: a) EMI-based clustering of ECa_z maps, b) combined EMI-

781 NDVI clustering with dataset-wise normalization (i.e., normalized by using the minimum and

782 maximum values for all the available data), and c) combined EMI-NDVI clustering with dataset-

783 wise normalization of EMI data and separate column-wise normalization of NDVI data. As

784 apparent in Figure A1b, the EMI measurements dominate the clustering results when an

785 inappropriate normalization is used. On the contrary, the normalization strategy used here (Figure

786 A1c) provides a clustering result where both EMI and NDVI meaningfully contribute.

787
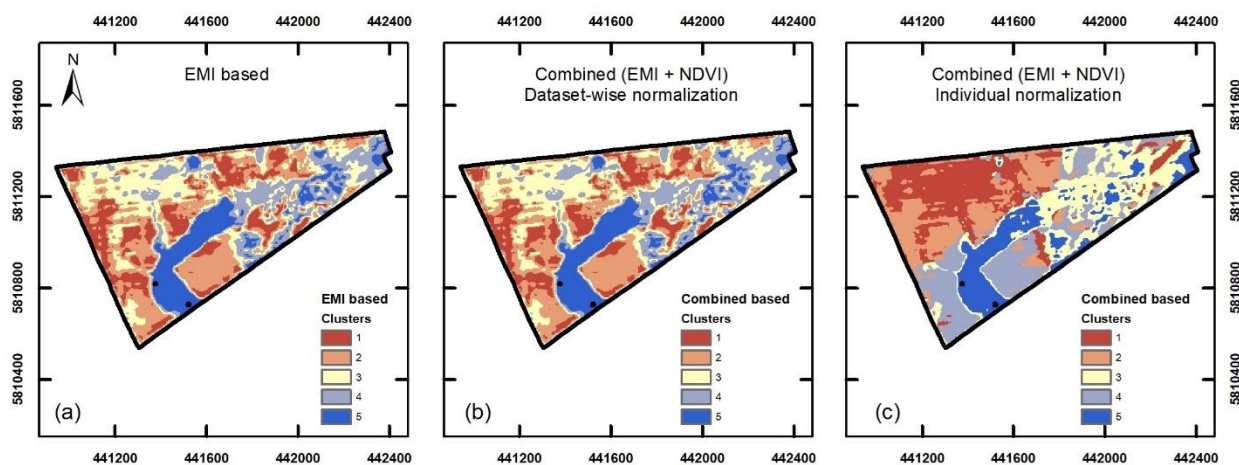
788 Figure A1. Comparison of management zone delineation using different normalization approaches

789 **(a)** EMI-based clustering without normalization, **(b)** Combined EMI and NDVI clustering with

790 dataset-wise normalization, **(c)** Combined EMI and NDVI clustering with individual

791 normalization, where EMI data were normalized as a dataset, while NDVI data were normalized

792 column-wise.

793

794

Appendix B: Additional results for post-hoc analysis

For the EMI dataset (VCP + HCP, 9 coils), the MCASD analysis suggested five clusters. The results of the post-hoc analysis are shown in Table B1. Statistically significant differences between two clusters are indicated by an *O* whereas an *X* indicates no significant differences. When two clusters have no statistically significant difference for any of the evaluated properties, they are merged. Therefore, clusters 4 and 5 were merged into a new cluster 4. For the NDVI dataset, the MCASD analysis suggested 4 clusters and the results of the post-hoc analysis (Table B2) merged clusters 3 and 4 into a new cluster 3. For the combined dataset (EMI + NDVI), the MCASD analysis suggested 4 clusters and the results of the post-hoc analysis (Table B3) merged clusters 1 and 2 into a new cluster 1.

Table B1. Post-hoc analysis of soil characteristics and yield for the EMI-based clusters leading to cluster merging. Statistically significant *(O)* or non-significant differences *(X)* are provided between clusters for soil texture, EOS layer, and yield.

Clusters		1vs2	2vs3	3vs4	4vs5
End of sandy layer (Depth cm)		*O*	*X*	*O*	*X*
Layer 1 (above EOS)	**Sand**	*X*	*O*	*O*	*X*
	Silt	*X*	*O*	*O*	*X*
	Clay	*X*	*O*	*O*	*X*
Layer 2 (below EOS)	**Sand**	*X*	*X*	*O*	*X*
	Silt	*X*	*X*	*O*	*X*
	Clay	*X*	*X*	*O*	*X*
Yield		*X*	*X*	*O*	*X*

810 Table B2. Post-hoc analysis of soil characteristics and yield for the NDVI-based clusters leading

811 to cluster merging. Statistically significant *(O)* or non-significant differences *(X)* are provided

812 between clusters for soil texture, EOS layer, and yield.

Clusters		1vs2	2vs3	3vs4
End of sandy layer (depth cm)		*X*	*O*	*X*
Layer 1 (above EOS)	**Sand**	*O*	*O*	*X*
	Silt	*O*	*O*	*X*
	Clay	*O*	*O*	*X*
Layer 2 (below EOS)	**Sand**	*X*	*O*	*X*
	Silt	*X*	*O*	*X*
	Clay	*X*	*O*	*X*
Yield		*X*	*O*	*X*

813

814 Table B3. Post-hoc analysis of soil characteristics and yield for the clusters based on EMI and

815 NDVI leading to cluster merging. Statistically significant *(O)* or non-significant differences *(X)*

816 are provided between clusters for soil texture, EOS layer, and yield.

Clusters		1vs2	2vs3	3vs4
End of sandy layer (depth cm)		*X*	*O*	*O*
Layer 1 (above EOS)	**Sand**	*X*	*O*	*O*
	Silt	*X*	*O*	*O*
	Clay	*X*	*O*	*O*
Layer 2 (below EOS)	**Sand**	*X*	*O*	*X*
	Silt	*X*	*O*	*X*
	Clay	*X*	*O*	*X*
Yield		*X*	*O*	*X*

817

 Appendix C: Differences in yield between derived management zones

819   Figure C1 presents boxplots illustrating yield variability (dt/ha) for two additional years: winter

820   rye in 2017 (Figure C1a) and rapeseed in 2018 (Figure C1b). Results are presented for management

821   zones derived from three clustering approaches: EMI-based (left), NDVI-based (middle), and

822   combined EMI + NDVI (right). These two years were selected as additional representative

823   examples, as the overall yield variation across the full nine-year dataset followed the same trend.

824   In the EMI-based management zones, yield distribution is relatively similar across the first three

825   zones, with a noticeable drop in the fourth zone. In contrast, NDVI-based and EMI + NDVI zones

826   show a progressive decline in yield across clusters, indicating a clearer trend of decreasing

827   productivity.

828

829
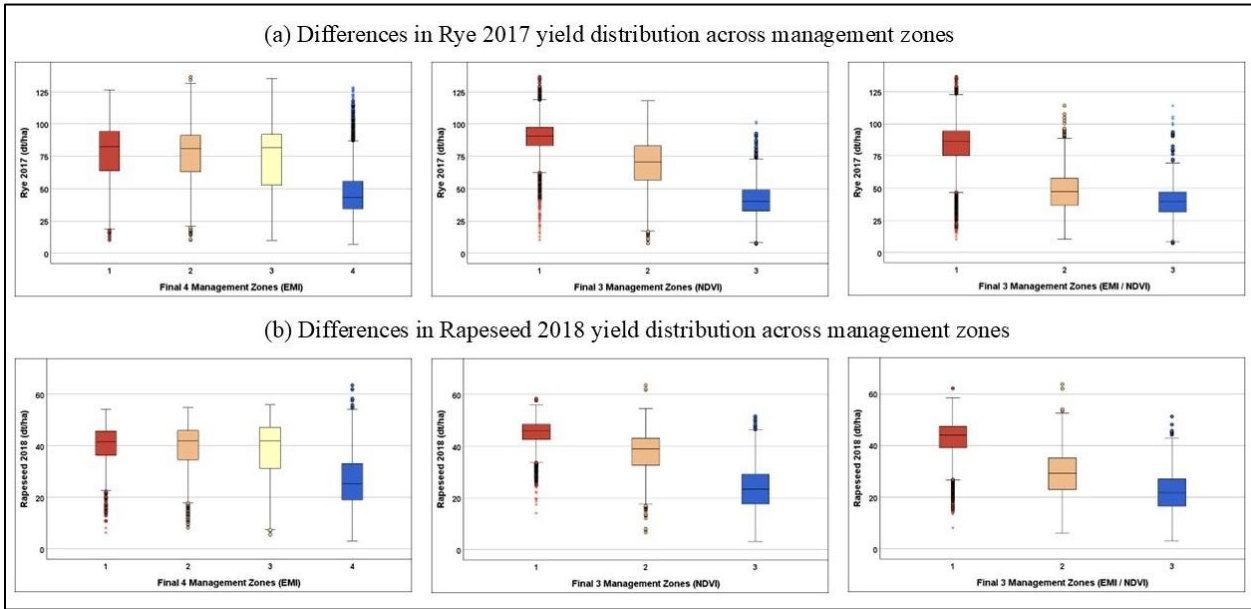
830   Figure C1. Yield distribution across final management zones based on EMI, NDVI, and

831   combined EMI-NDVI datasets.

Data availability

The data that support the findings of this study are available on request from the corresponding author.

Author contributions

SD, CB, and JH: conceptualization and methodology; SD, CB, MD, and IO: field measurements; SD, MD, DL and CB: data analysis; SD: writing – original draft; CB, DL, IO, MD, HV, and JH: writing: review and editing; JH – project supervision. All authors have read and agreed to the published version of the manuscript.

Competing interest

A co-author (Dave O'Leary) of this article is a member of the guest editorial board for this Special Issue: "Agrogeophysics: illuminating soil's hidden dimensions".

Special issue statement

This article is part of the special issue "Agrogeophysics: illuminating soil's hidden dimensions". It is not associated with a conference.

Acknowledgements

We thank Dr. agr. Kathrin Grahmann, Robert Zieciak, Anna Engels, Tawhid Hossain for local support, organizational formalities and data. Danial Mansourian, Ali Chaudhry, Emilio Capitanio, Dr. Muhammad Fahad, and Ali Sadrzadeh are thanked for their help during the EMI measurement

854   campaigns. The maintenance of the patchCROP infrastructure is supported by the Leibniz Centre

855   for Agricultural Landscape Research.

856

857   **Financial support**

858   This research was supported by the DFG (German Research Foundation) through the Germany's

859   Excellence Strategy EXC 2070, Grant No. 390732324 - PhenoRob. Additionally, the infrastructure

860   used for EMI measurements in this research was supported by funding through the BMBF

861   BioökonomieREVIER funding scheme with its "BioRevierPlus" project (funding ID: 031B1137D

862   / 031B1137DX).

References

Abdu, H., Robinson, D. A., Seyfried, M., and Jones, S. B.: Geophysical imaging of watershed subsurface patterns and prediction of soil texture and water holding capacity, Water Resour. Res., 44, 1–10, https://doi.org/10.1029/2008wr007043, 2008.

Adamchuk, V., Allred, B., Doolittle, J., Grote, K., and Viscarra Rossel, R. A.: Tools for proximal soil sensing, Soil Surv. Man. soil Sci. Div. Staff. Washington, DC United States Dep. Agric., 355–356, 2017.

Adhikari, K., Smith, D. R., Collins, H., Hajda, C., Acharya, B. S., and Owens, P. R.: Mapping Within-Field Soil Health Variations Using Apparent Electrical Conductivity, Topography, and Machine Learning, Agronomy, 12, 1–16, https://doi.org/10.3390/agronomy12051019, 2022.

Ali, A., Rondelli, V., Martelli, R., Falsone, G., Lupia, F., and Barbanti, L.: Management Zones Delineation through Clustering Techniques Based on Soils Traits, NDVI Data, and Multiple Year Crop Yields, Agric., 12, https://doi.org/10.3390/agriculture12020231, 2022.

Altdorff, D., von Hebel, C., Borchard, N., van der Kruk, J., Bogena, H. R., Vereecken, H., and Huisman, J. A.: Potential of catchment-wide soil water content prediction using electromagnetic induction in a forest ecosystem, Environ. Earth Sci., 76, 1–11, https://doi.org/10.1007/s12665-016-6361-3, 2017.

de Amorim, L. B. V., Cavalcanti, G. D. C., and Cruz, R. M. O.: The choice of scaling technique matters for classification performance, Appl. Soft Comput., 133, 1–37, https://doi.org/10.1016/j.asoc.2022.109924, 2023.

patchCROP: https://comm.zalf.de/sites/patchcrop/SitePages/Homepage.aspx, last access: 25 June 2025.

Antle, J. M., Basso, B., Conant, R. T., Godfray, H. C. J., Jones, J. W., Herrero, M., Howitt, R. E.,

886   Keating, B. A., Munoz-Carpena, R., Rosenzweig, C., Tittonell, P., and Wheeler, T. R.: Towards

887   a new generation of agricultural system data, models and knowledge products: Design and

888   improvement, Agric. Syst., 155, 255–268, https://doi.org/10.1016/j.agsy.2016.10.002, 2017.

889   Arshad, M. A. C., Lowery, B., and Grossman, B.: Physical Tests for Monitoring Soil Quality,

890   123–141, https://doi.org/10.2136/sssaspecpub49.c7, 2015.

891   Becker, S. M., Franz, T. E., Abimbola, O., Steele, D. D., Flores, J. P., Jia, X., Scherer, T. F.,

892   Rudnick, D. R., and Neale, C. M. U.: Feasibility assessment on use of proximal geophysical

893   sensors to support precision management, Vadose Zo. J., 21, 1–18,

894   https://doi.org/10.1002/vzj2.20228, 2022.

895   Bijeesh, T. V. and Narasimhamurthy, K. N.: Surface water detection and delineation using

896   remote sensing images: a review of methods and algorithms, Sustain. Water Resour. Manag., 6,

897   1–23, https://doi.org/10.1007/s40899-020-00425-4, 2020.

898   Binley, A., Hubbard, S. S., Huisman, J. a, Revil, A., Robinson, D. a, Singha, K., and Slater, L.

899   D.: The emergence of hydrogeophysics for improved understanding of subsurface processes over

900   multiple scales, Water Resour. Res., 51, 3837–3866, https://doi.org/10.1002/2015WR017016,

901   2015.

902   Blanchy, G., McLachlan, P., Mary, B., Censini, M., Boaga, J., and Cassiani, G.: Comparison of

903   multi-coil and multi-frequency frequency domain electromagnetic induction instruments, Front.

904   Soil Sci., 4, 1–13, https://doi.org/10.3389/fsoil.2024.1239497, 2024.

905   Bongiovanni, R. and Lowenberg-Deboer, J.: Precision agriculture and sustainability, Precis.

906   Agric., 5, 359–387, https://doi.org/10.1023/B:PRAG.0000040806.39604.aa, 2004.

907   Breunig, F. M., Galvão, L. S., Dalagnol, R., Dauve, C. E., Parraga, A., Santi, A. L., Della Flora,

908   D. P., and Chen, S.: Delineation of management zones in agricultural fields using cover–crop

909   biomass estimates from PlanetScope data, Int. J. Appl. Earth Obs. Geoinf., 85,

910   https://doi.org/10.1016/j.jag.2019.102004, 2020.

911   Brogi, C., Huisman, J. A., Pätzold, S., von Hebel, C., Weihermüller, L., Kaufmann, M. S., van

912   der Kruk, J., and Vereecken, H.: Large-scale soil mapping using multi-configuration EMI and

913   supervised image classification, Geoderma, 335, 133–148,

914   https://doi.org/10.1016/j.geoderma.2018.08.001, 2019.

915   Brogi, C., Huisman, J. A., Weihermüller, L., Herbst, M., and Vereecken, H.: Added value of

916   geophysics-based soil mapping in agro-ecosystem simulations, Soil, 7, 125–143,

917   https://doi.org/10.5194/soil-7-125-2021, 2021.

918   Carfagna, E. and Gallego, F. J.: Using remote sensing for agricultural statistics, Int. Stat. Rev.,

919   73, 389–404, https://doi.org/10.1111/j.1751-5823.2005.tb00155.x, 2005.

920   Castrignanò, A., Buttafuoco, G., Quarto, R., Parisi, D., Viscarra Rossel, R. A., Terribile, F.,

921   Langella, G., and Venezia, A.: A geostatistical sensor data fusion approach for delineating

922   homogeneous management zones in Precision Agriculture, Catena, 167, 293–304,

923   https://doi.org/10.1016/j.catena.2018.05.011, 2018.

924   Celebi, M. E., Kingravi, H. A., and Vela, P. A.: A comparative study of efficient initialization

925   methods for the k-means clustering algorithm, Expert Syst. Appl., 40, 200–210,

926   https://doi.org/10.1016/j.eswa.2012.07.021, 2013.

927   Chartzoulakis, K. and Bertaki, M.: Sustainable Water Management in Agriculture under Climate

928   Change, Agric. Agric. Sci. Procedia, 4, 88–98, https://doi.org/10.1016/j.aaspro.2015.03.011,

929   2015.

930   Chlingaryan, A., Sukkarieh, S., and Whelan, B.: Machine learning approaches for crop yield

931   prediction and nitrogen status estimation in precision agriculture: A review, Comput. Electron.

Agric., 151, 61–69, https://doi.org/10.1016/j.compag.2018.05.012, 2018.

Ciampalini, A., André, F., Garfagnoli, F., Grandjean, G., Lambot, S., Chiarantini, L., and

Moretti, S.: Improved estimation of soil clay content by the fusion of remote hyperspectral and

proximal geophysical sensing, J. Appl. Geophys., 116, 135–145,

https://doi.org/10.1016/j.jappgeo.2015.03.009, 2015.

Corwin, D. L. and Lesch, S. M.: Application of soil electrical conductivity to precision

agriculture: Theory, principles, and guidelines, Agron. J., 95, 455–471,

https://doi.org/10.2134/agronj2003.4550, 2003.

Corwin, D. L. and Lesch, S. M.: Apparent soil electrical conductivity measurements in

agriculture, Comput. Electron. Agric., 46, 11–43, https://doi.org/10.1016/j.compag.2004.10.005,

2005.

Corwin, D. L. and Scudiero, E.: Review of soil salinity assessment for agriculture across

multiple scales using proximal and/or remote sensors, Adv. Agron., 158, 1–130,

https://doi.org/10.1016/BS.AGRON.2019.07.001, 2019.

Dobarco, M. R., McBratney, A., Minasny, B., and Malone, B.: A framework to assess changes in

soil condition and capability over large areas, Soil Secur., 4,

https://doi.org/10.1016/j.soisec.2021.100011, 2021.

Donat, M., Geistert, J., Grahmann, K., Bloch, R., and Bellingrath-Kimura, S. D.: Patch cropping-

a new methodological approach to determine new field arrangements that increase the

multifunctionality of agricultural landscapes, Comput. Electron. Agric., 197, 106894,

https://doi.org/10.1016/j.compag.2022.106894, 2022.

DWD: Deutscher Wetterdienst (DWD) Climate Data Center (CDC): Monatssumme der

Stationsmessungen der Niederschlagshöhe in mm für Deutschland, Version v21.3, Deutscher

955   Wetterdienst, 2021.

956   ESRI: Esri, Maxar, Earthstar Geographics, and the GIS User Community, 2020.

957   Esteves, C., Fangueiro, D., Braga, R. P., Martins, M., Botelho, M., and Ribeiro, H.: Assessing

958   the Contribution of ECa and NDVI in the Delineation of Management Zones in a Vineyard,

959   Agronomy, 12, https://doi.org/10.3390/agronomy12061331, 2022.

960   Garré, S., Hyndman, D., Mary, B., and Werban, U.: Geophysics conquering new territories: The

961   rise of "agrogeophysics," Vadose Zo. J., 20, 2–5, https://doi.org/10.1002/vzj2.20115, 2021.

962   Gebbers, R. and Adamchuk, V. I.: Precision Agriculture and Food Security, Science (80-.)., 327,

963   828–831, https://doi.org/10.1126/science.1183899, 2010.

964   Geng, X., Mu, Y., Mao, S., Ye, J., and Zhu, L.: An Improved K-Means Algorithm Based on

965   Fuzzy Metrics, IEEE Access, 8, 217416–217424,

966   https://doi.org/10.1109/ACCESS.2020.3040745, 2020.

967   Georgi, C., Spengler, D., Itzerott, S., and Kleinschmit, B.: Automatic delineation algorithm for

968   site-specific management zones based on satellite remote sensing data, Precis. Agric., 19, 684–

969   707, https://doi.org/10.1007/s11119-017-9549-y, 2018.

970   Grahmann, K., Reckling, M., Hernandez-Ochoa, I., and Ewert, F.: Intercropping for

971   sustainability: Research developments and their application An agricultural diversification trial

972   by patchy field arrangements at the landscape level: The landscape living lab "patchCROP,"

973   Asp. Appl. Biol., 146, 2021, 2021.

974   Grahmann, K., Reckling, M., Hernández-Ochoa, I., Donat, M., Bellingrath-Kimura, S., and

975   Ewert, F.: Co-designing a landscape experiment to investigate diversified cropping systems,

976   Agric. Syst., 217, https://doi.org/10.1016/j.agsy.2024.103950, 2024.

977   Hamidov, A., Helming, K., Bellocchi, G., Bojar, W., Dalgaard, T., Ghaley, B. B., Hoffmann, C.,

978 Holman, I., Holzkämper, A., Krzeminska, D., Kværnø, S. H., Lehtonen, H., Niedrist, G.,

979 Øygarden, L., Reidsma, P., Roggero, P. P., Rusu, T., Santos, C., Seddaiu, G., Skarbøvik, E.,

980 Ventrella, D., Żarski, J., and Schönhart, M.: Impacts of climate change adaptation options on soil

981 functions: A review of European case-studies, L. Degrad. Dev., 29, 2378–2389,

982 https://doi.org/10.1002/ldr.3006, 2018.

983 Hatfield, J. L. and Prueger, J. H.: Value of using different vegetative indices to quantify

984 agricultural crop characteristics at different growth stages under varying management practices,

985 Remote Sens., 2, 562–578, https://doi.org/10.3390/rs2020562, 2010.

986 von Hebel, C., Rudolph, S., Mester, A., Huisman, J. A., Kumbhar, P., Vereecken, H., and van

987 der Kruk, J.: Three-dimensional imaging of subsurface structural patterns using quantitative

988 large-scale multiconfiguration electromagnetic induction data, Water Resour. Res., 50, 2732–

989 2748, https://doi.org/10.1002/2013WR014864, 2014.

990 von Hebel, C., Matveeva, M., Verweij, E., Rademske, P., Kaufmann, M. S., Brogi, C.,

991 Vereecken, H., Rascher, U., and van der Kruk, J.: Understanding Soil and Plant Interaction by

992 Combining Ground-Based Quantitative Electromagnetic Induction and Airborne Hyperspectral

993 Data, Geophys. Res. Lett., 45, 7571–7579, https://doi.org/10.1029/2018GL078658, 2018.

994 von Hebel, C., Reynaert, S., Pauly, K., Janssens, P., Piccard, I., Vanderborght, J., van der Kruk,

995 J., Vereecken, H., and Garré, S.: Toward high-resolution agronomic soil information and

996 management zones delineated by ground-based electromagnetic induction and aerial drone data,

997 Vadose Zo. J., 20, 1–18, https://doi.org/10.1002/vzj2.20099, 2021.

998 Hernández-Ochoa, I. M., Gaiser, T., Grahmann, K., Engels, A., Kersebaum, K. C., Seidel, S. J.,

999 and Ewert, F.: Cross model validation for a diversified cropping system, Eur. J. Agron., 157,

1000 https://doi.org/10.1016/j.eja.2024.127181, 2024.

1001 Hou, D., Bolan, N. S., Tsang, D. C. W., Kirkham, M. B., and O'Connor, D.: Sustainable soil use

1002 and management: An interdisciplinary and systematic approach, Sci. Total Environ., 729,

1003 138961, https://doi.org/10.1016/j.scitotenv.2020.138961, 2020.

1004 Hunt, M. L., Blackburn, G. A., Carrasco, L., Redhead, J. W., and Rowland, C. S.: High

1005 resolution wheat yield mapping using Sentinel-2, Remote Sens. Environ., 233, 111410,

1006 https://doi.org/10.1016/j.rse.2019.111410, 2019.

1007 ISO, D.: 11277: 2002-08, Soil Qual. Part. size Distrib. Miner. soil Mater. method by sieving

1008 Sediment., https://doi.org/10.31030/9283499, 2002.

1009 IUSS Working Group: International soil classification system for naming soils and creating

1010 legends for soil maps, World Soil Resour. Reports, 106, 166–168, 2015.

1011 Jadoon, K. Z., Moghadas, D., Jadoon, A., Missimer, T. M., Al-Mashharawi, S. K., and McCabe,

1012 M. F.: Estimation of soil salinity in a drip irrigation system by using joint inversion of multicoil

1013 electromagnetic induction measurements, Water Resour. Res., 51, 3490–3504,

1014 https://doi.org/10.1002/2014WR016245, 2015.

1015 James, I. T., Waine, T. W., Bradley, R. I., Taylor, J. C., and Godwin, R. J.: Determination of Soil

1016 Type Boundaries using Electromagnetic Induction Scanning Techniques, Biosyst. Eng., 86, 421–

1017 430, https://doi.org/10.1016/j.biosystemseng.2003.09.001, 2003.

1018 Janrao, P., Mishra, D., and Bharadi, V.: Clustering Approaches for Management Zone

1019 Delineation in Precision Agriculture for Small Farms, SSRN Electron. J., 1347–1356,

1020 https://doi.org/10.2139/ssrn.3356457, 2019.

1021 Jin, Z., Azzari, G., You, C., Di Tommaso, S., Aston, S., Burke, M., and Lobell, D. B.:

1022 Smallholder maize area and yield mapping at national scales with Google Earth Engine, Remote

1023 Sens. Environ., 228, 115–128, https://doi.org/10.1016/j.rse.2019.04.016, 2019.

1024   Kaufmann, M. S., von Hebel, C., Weihermüller, L., Baumecker, M., Döring, T., Schweitzer, K.,

1025   Hobley, E., Bauke, S. L., Amelung, W., Vereecken, H., and van der Kruk, J.: Effect of fertilizers

1026   and irrigation on multi-configuration electromagnetic induction measurements, Soil Use Manag.,

1027   36, 104–116, https://doi.org/10.1111/sum.12530, 2020.

1028   Kaya, F., Ferhatoglu, C., and Başayiğit, L.: Multi-Temporal Normalized Difference Vegetation

1029   Index Based on High Spatial Resolution Satellite Images Reveals Insight-Driven Edaphic

1030   Management Zones, AgriEngineering, 7, https://doi.org/10.3390/agriengineering7040092, 2025.

1031   Keller, G. . and Frischknecht, F. .: Electrical Methods in Geophysical Propecting, Oxford, New

1032   York, Pergamon Press, 1966.

1033   Khan, S., Tufail, M., Khan, M. T., Khan, Z. A., Iqbal, J., and Alam, M.: A novel semi-supervised

1034   framework for UAV based crop/weed classification, PLoS One, 16,

1035   https://doi.org/10.1371/journal.pone.0251008, 2021.

1036   Kibblewhite, M. G., Ritz, K., and Swift, M. J.: Soil health in agricultural systems, Philos. Trans.

1037   R. Soc. B Biol. Sci., 363, 685–701, https://doi.org/10.1098/rstb.2007.2178, 2008.

1038   Koch, T., Deumlich, D., Chifflard, P., Panten, K., and Grahmann, K.: Using model simulation to

1039   evaluate soil loss potential in diversified agricultural landscapes, Eur. J. Soil Sci., 74, 1–14,

1040   https://doi.org/10.1111/ejss.13332, 2023.

1041   Koganti, T., De Smedt, P., Farzamian, M., Knadel, M., Triantafilis, J., Christiansen, A. V., and

1042   Greve, M. H.: Editorial: Digital soil mapping using electromagnetic sensors, Front. Soil Sci., 4,

1043   10–12, https://doi.org/10.3389/fsoil.2024.1536797, 2024.

1044   Kohonen, T.: Essentials of the self-organizing map, Neural Networks, 37, 52–65,

1045   https://doi.org/10.1016/j.neunet.2012.09.018, 2013.

1046   Kuang, B., Mahmood, H. S., Quraishi, M. Z., Hoogmoed, W. B., Mouazen, A. M., and van

1047 Henten, E. J.: Sensing Soil Properties in the Laboratory, In Situ, and On-Line, 155–223,

1048 https://doi.org/10.1016/B978-0-12-394275-3.00003-1, 2012.

1049 Lavoué, F., Van Der Kruk, J., Rings, J., André, F., Moghadas, D., Huisman, J. A., Lambot, S.,

1050 LWeihermüller, Vanderborght, J., and Vereecken, H.: Electromagnetic induction calibration

1051 using apparent electrical conductivity modelling based on electrical resistivity tomography, Near

1052 Surf. Geophys., 8, 553–561, https://doi.org/10.3997/1873-0604.2010037, 2010.

1053 Li, Y., Ni, Z., Jin, F., Li, J., and Li, F.: Research on Clustering Method of Improved Glowworm

1054 Algorithm Based on Good-Point Set, Math. Probl. Eng., 2018,

1055 https://doi.org/10.1155/2018/8724084, 2018.

1056 Liaghat, S. and Balasundram, S. K.: A review: The role of remote sensing in precision

1057 agriculture, Am. J. Agric. Biol. Sci., 5, 50–55, https://doi.org/10.3844/ajabssp.2010.50.55, 2010.

1058 Liakos, K. G., Busato, P., Moshou, D., Pearson, S., and Bochtis, D.: Machine learning in

1059 agriculture: A review, Sensors (Switzerland), 18, 1–29, https://doi.org/10.3390/s18082674, 2018.

1060 Liang, J., Zhao, X., Li, D., Cao, F., and Dang, C.: Determining the number of clusters using

1061 information entropy for mixed data, Pattern Recognit., 45, 2251–2265,

1062 https://doi.org/10.1016/j.patcog.2011.12.017, 2012.

1063 Licker, R., Johnston, M., Foley, J. A., Barford, C., Kucharik, C. J., Monfreda, C., and

1064 Ramankutty, N.: Mind the gap: How do climate and agricultural management explain the "yield

1065 gap" of croplands around the world?, Glob. Ecol. Biogeogr., 19, 769–782,

1066 https://doi.org/10.1111/j.1466-8238.2010.00563.x, 2010.

1067 López-Granados, F.: Weed detection for site-specific weed management: mapping and real-time

1068 approaches, Weed Res., 51, 1–11, https://doi.org/10.1111/j.1365-3180.2010.00829.x, 2011.

1069 Lueck, E. and Ruehlmann, J.: Resistivity mapping with GEOPHILUS ELECTRICUS -

1070   Information about lateral and vertical soil heterogeneity, Geoderma, 199, 2–11,

1071   https://doi.org/10.1016/j.geoderma.2012.11.009, 2013.

1072   McNeill, J. D.: Electromagnetic Terrain Conductivity Measurement at Low Induction Numbers,

1073   https://geonics.com/pdfs/technicalnotes/tn6.pdf, 1980.

1074   Meyer, S., Kling, C., Vogel, S., Schröter, I., Nagel, A., Kramer, E., Gebbers, R., Philipp, G.,

1075   Lück, K., Gerlach, F., Scheibe, D., and Ruehlmann, J.: Creating soil texture maps for precision

1076   liming using electrical resistivity and gamma ray mapping, in: Precision agriculture '19, 539–

1077   546, https://doi.org/10.3920/978-90-8686-888-9_67, 2019.

1078   Mohammed, I., Marshall, M., de Bie, K., Estes, L., and Nelson, A.: A blended census and

1079   multiscale remote sensing approach to probabilistic cropland mapping in complex landscapes,

1080   ISPRS J. Photogramm. Remote Sens., 161, 233–245,

1081   https://doi.org/10.1016/j.isprsjprs.2020.01.024, 2020.

1082   Moshou, D., Bravo, C., Wahlen, S., West, J., McCartney, A., De Baerdemaeker, J., and Ramon,

1083   H.: Simultaneous identification of plant stresses and diseases in arable crops using proximal

1084   optical sensing and self-organising maps, Precis. Agric., 7, 149–164,

1085   https://doi.org/10.1007/s11119-006-9002-0, 2006.

1086   Geologischer Dienst NRW: https://www.gd.nrw.de/.

1087   O'Leary, D., Brown, C., Healy, M. G., Regan, S., and Daly, E.: Observations of intra-peatland

1088   variability using multiple spatially coincident remotely sensed data sources and machine

1089   learning, Geoderma, 430, 116348, https://doi.org/10.1016/j.geoderma.2023.116348, 2023.

1090   O'Leary, D., Brogi, C., Brown, C., Tuohy, P., and Daly, E.: Linking electromagnetic induction

1091   data to soil properties at field scale aided by neural network clustering, Front. Soil Sci., 4, 1–13,

1092   https://doi.org/10.3389/fsoil.2024.1346028, 2024.

Öttl, L. K., Wilken, F., Auerswald, K., Sommer, M., Wehrhan, M., and Fiener, P.: Tillage

erosion as an important driver of in-field biomass patterns in an intensively used hummocky

landscape, L. Degrad. Dev., 32, 3077–3091, https://doi.org/10.1002/ldr.3968, 2021.

Patro, S. G. K. and sahu, K. K.: Normalization: A Preprocessing Stage, Iarjset, 20–22,

https://doi.org/10.17148/iarjset.2015.2305, 2015.

Pedregosa, F., Varoquaux, G., Gramfort, A., Michel, V., Thirion, B., Grisel, O., Blondel, M.,

Müller, A., Nothman, J., Louppe, G., Prettenhofer, P., Weiss, R., Dubourg, V., Vanderplas, J.,

Passos, A., Cournapeau, D., Brucher, M., Perrot, M., and Duchesnay, É.: Scikit-learn: Machine

Learning in Python, J. Mach. Learn. Res., 12, 2825–2830,

https://doi.org/10.48550/arXiv.1201.0490, 2011.

Pedrera-Parrilla, A., Brevik, E. C., Giráldez, J. V., and Vanderlinden, K.: Temporal stability of

electrical conductivity in a sandy soil, Int. Agrophysics, 30, 349–357,

https://doi.org/10.1515/intag-2016-0005, 2016.

Pradipta, A., Soupios, P., Kourgialas, N., Doula, M., Dokou, Z., Makkawi, M., Alfarhan, M.,

Tawabini, B., and Kirmizakis, P.: Precision Agriculture — Part 1 : Soil Applications, Water, 14,

1158., 2022.

Robinet, J., von Hebel, C., Govers, G., van der Kruk, J., Minella, J. P. G., Schlesner, A.,

Ameijeiras-Mariño, Y., and Vanderborght, J.: Spatial variability of soil water content and soil

electrical conductivity across scales derived from Electromagnetic Induction and Time Domain

Reflectometry, Geoderma, 314, 160–174, https://doi.org/10.1016/j.geoderma.2017.10.045, 2018.

Romero-Ruiz, A., O'Leary, D., Daly, E., Tuohy, P., Milne, A., Coleman, K., and Whitmore, A.

P.: An agrogeophysical modelling framework for the detection of soil compaction spatial

variability due to grazing using field-scale electromagnetic induction data, Soil Use Manag., 40,

https://doi.org/10.1111/sum.13039, 2024.

Rudolph, S., van der Kruk, J., von Hebel, C., Ali, M., Herbst, M., Montzka, C., Pätzold, S., Robinson, D. A., Vereecken, H., and Weihermüller, L.: Linking satellite derived LAI patterns with subsoil heterogeneity using large-scale ground-based electromagnetic induction measurements, Geoderma, 241–242, 262–271, https://doi.org/10.1016/j.geoderma.2014.11.015, 2015.

Saifuzzaman, M., Adamchuk, V., Buelvas, R., Biswas, A., Prasher, S., Rabe, N., Aspinall, D., and Ji, W.: Clustering tools for integration of satellite remote sensing imagery and proximal soil sensing data, Remote Sens., 11, 1–17, https://doi.org/10.3390/rs11091036, 2019.

Saputra, Danny Matthew, SAPUTRA, D., and OSWARI, L. D.: Effect of Distance Metrics in Determining K-Value in K-Means Clustering Using Elbow and Silhouette Method, 172, 341–346, https://doi.org/10.2991/aisr.k.200424.051, 2020.

Schmäck, J., Weihermüller, L., Klotzsche, A., von Hebel, C., Pätzold, S., Welp, G., and Vereecken, H.: Large-scale detection and quantification of harmful soil compaction in a post-mining landscape using multi-configuration electromagnetic induction, Soil Use Manag., 38, 212–228, https://doi.org/10.1111/sum.12763, 2022.

Schubert, E.: Stop using the elbow criterion for k-means and how to choose the number of clusters instead, ACM SIGKDD Explor. Newsl., 25, 36–42, https://doi.org/10.1145/3606274.3606278, 2023.

Scudiero, E., Teatini, P., Manoli, G., Braga, F., Skaggs, T. H., and Morari, F.: Workflow to establish time-specific zones in precision agriculture by spatiotemporal integration of plant and soil sensing data, Agronomy, 8, 1–21, https://doi.org/10.3390/agronomy8110253, 2018.

Simpson, D., Lehouck, A., Verdonck, L., Vermeersch, H., Van Meirvenne, M., Bourgeois, J.,

Thoen, E., and Docter, R.: Comparison between electromagnetic induction and fluxgate gradiometer measurements on the buried remains of a 17th century castle, J. Appl. Geophys., 68, 294–300, https://doi.org/10.1016/j.jappgeo.2009.03.006, 2009.

Sishodia, R. P., Ray, R. L., and Singh, S. K.: Applications of remote sensing in precision agriculture: A review, Remote Sens., 12, 1–31, https://doi.org/10.3390/rs12193136, 2020.

Skakun, S., Kalecinski, N. I., Brown, M. G. L., Johnson, D. M., Vermote, E. F., Roger, J. C., and Franch, B.: Assessing within-field corn and soybean yield variability from worldview-3, planet, sentinel-2, and landsat 8 satellite imagery, Remote Sens., 13, 1–18, https://doi.org/10.3390/rs13050872, 2021.

Stamford, J. D., Vialet-Chabrand, S., Cameron, I., and Lawson, T.: Development of an accurate low cost NDVI imaging system for assessing plant health, Plant Methods, 19, 1–19, https://doi.org/10.1186/s13007-023-00981-8, 2023.

Tagarakis, A., Liakos, V., Fountas, S., Koundouras, S., and Gemtos, T. A.: Management zones delineation using fuzzy clustering techniques in grapevines, Precis. Agric., 14, 18–39, https://doi.org/10.1007/s11119-012-9275-4, 2013.

Taşdemir, K., Milenov, P., and Tapsall, B.: A hybrid method combining SOM-based clustering and object-based analysis for identifying land in good agricultural condition, Comput. Electron. Agric., 83, 92–101, https://doi.org/10.1016/j.compag.2012.01.017, 2012.

Trivedi, M. B., Marshall, M., Estes, L., de Bie, C. A. J. M., Chang, L., and Nelson, A.: Cropland Mapping in Tropical Smallholder Systems with Seasonally Stratified Sentinel-1 and Sentinel-2 Spectral and Textural Features, Remote Sens., 15, https://doi.org/10.3390/rs15123014, 2023.

Do you know all 17 SDGs? (2021): https://sdgs.un.org/goals.

Usama, M., Qadir, J., Raza, A., Arif, H., Yau, K. L. A., Elkhatib, Y., Hussain, A., and Al-

1162 Fuqaha, A.: Unsupervised Machine Learning for Networking: Techniques, Applications and

1163 Research Challenges, IEEE Access, 7, 65579–65615,

1164 https://doi.org/10.1109/ACCESS.2019.2916648, 2019.

1165 Valentine, A. and Kalnins, L.: An introduction to learning algorithms and potential applications

1166 in geomorphometry and Earth surface dynamics, Earth Surf. Dyn., 4, 445–460,

1167 https://doi.org/10.5194/esurf-4-445-2016, 2016.

1168 Vogel, S., Gebbers, R., Oertel, M., and Kramer, E.: Evaluating soil-borne causes of biomass

1169 variability in Grassland by remote and proximal sensing, Sensors (Switzerland), 19, 1–16,

1170 https://doi.org/10.3390/s19204593, 2019.

1171 Wang, F., Yang, S., Wei, Y., Shi, Q., and Ding, J.: Characterizing soil salinity at multiple depth

1172 using electromagnetic induction and remote sensing data with random forests: A case study in

1173 Tarim River Basin of southern Xinjiang, China, Sci. Total Environ., 754, 142030,

1174 https://doi.org/10.1016/j.scitotenv.2020.142030, 2021.

1175 Wang, L., Duan, Y., Zhang, L., Rehman, T. U., Ma, D., and Jin, J.: Precise estimation of NDVI

1176 with a simple NIR sensitive RGB camera and machine learning methods for corn plants, Sensors

1177 (Switzerland), 20, 1–15, https://doi.org/10.3390/s20113208, 2020.

1178 Ward, S. H. and Hohmann, G. W.: 4. Electromagnetic Theory for Geophysical Applications, in:

1179 Electromagnetic Methods in Applied Geophysics, Society of Exploration Geophysicists, 130–

1180 311, https://doi.org/10.1190/1.9781560802631.ch4, 1988.

1181 Weiss, M., Jacob, F., and Duveiller, G.: Remote sensing for agricultural applications: A meta-

1182 review, Remote Sens. Environ., 236, 111402, https://doi.org/10.1016/j.rse.2019.111402, 2020.

1183 Wilhelm, W. W., Ruwe, K., and Schlemmer, M. R.: Comparison of three leaf area index meters

1184 in a corn canopy, Crop Sci., 40, 1179–1183, https://doi.org/10.2135/cropsci2000.4041179x,

2000.

Xue, J. and Su, B.: Significant remote sensing vegetation indices: A review of developments and applications, J. Sensors, 2017, https://doi.org/10.1155/2017/1353691, 2017.

Ylagan, S., Brye, K. R., Ashworth, A. J., Owens, P. R., Smith, H., and Poncet, A. M.: Using Apparent Electrical Conductivity to Delineate Field Variation in an Agroforestry System in the Ozark Highlands, Remote Sens., 14, 1–25, https://doi.org/10.3390/rs14225777, 2022.

Zhang, Y. and Wang, Y.: Machine learning applications for multi-source data of edible crops: A review of current trends and future prospects, Food Chem. X, 19, 100860, https://doi.org/10.1016/j.fochx.2023.100860, 2023.

Zhu, Q., Lin, H., and Doolittle, J.: Repeated Electromagnetic Induction Surveys for Determining Subsurface Hydrologic Dynamics in an Agricultural Landscape, Soil Sci. Soc. Am. J., 74, 1750–1762, https://doi.org/10.2136/sssaj2010.0055, 2010.